Author/s:
Fehrmann, J;Belleville, B;Ozarska, B;Ismayati, M;Dwianto, W

Title:
Effects of mat composition and pressing time on citric acid-bonded ultra-low-density hemp hurd particleboard

Date:
2024-04-01

Citation:
Fehrmann, J., Belleville, B., Ozarska, B., Ismayati, M. & Dwianto, W. (2024). Effects of mat composition and pressing time on citric acid-bonded ultra-low-density hemp hurd particleboard. Industrial Crops and Products, 210, https://doi.org/10.1016/j.indcrop.2024.118070.

Persistent Link:
https://hdl.handle.net/11343/340093

Industrial Crops & Products 210 (2024) 118070

Contents lists available at ScienceDirect

Industrial Crops & Products

journal homepage: www.elsevier.com/locate/indcrop

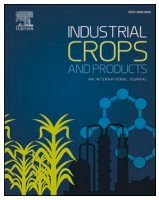

Effects of mat composition and pressing time on citric acid-bonded ultra-low-density hemp hurd particleboard

Johannes Fehrmann [a,*], Benoit Belleville [a], Barbara Ozarska [a], Maya Ismayati [b], Wahyu Dwianto [b]

[a] The University of Melbourne, Australia
[b] National Research and Innovation Agency (BRIN), Indonesia

ARTICLE INFO

Keywords:
Hemp hurd
Citric acid
Agricultural by-products
Ultra-low density particleboard
Thermo-chemical properties
Physico-mechanical properties

ABSTRACT

This study investigated the feasibility of using citric acid (CA) as a biobased and formaldehyde-free binder for producing ultra-low-density (320 to 338 kg/m^3) hemp hurd particleboard (ULHPB). Mechanically decorticated hemp hurd chips were milled and then separated into fine (F), medium (M), and coarse (C) particle sizes. Three particle size mixes (PSM) were used to fabricate the panels: 100% C, 100% M, and a 50/50% mixture of CM. Each PSM was combined with *low* and *high* CA contents (20 and 30 wt%) and subjected to *short* and *long* pressing times (8 and 12 min) at 200 °C. Physico-mechanical characteristics were evaluated following Australian standard AS/NZS 1859.1 (2017) for reconstituted wood-based panels. Thermo-chemical analyses were performed to understand the properties of the raw hurd and to investigate the binding mechanisms in CA-ULHPB. The PSM had a significant impact on panel expansion (springback), internal bond strength (IB), water absorption (WA), and thickness swelling (TS) in most CA-ULHPB variants. PSM-C panels exhibited superior IB when pressed with 30 wt% CA for 12 min. The effect of PSMs diminished for WA and TS but CA content and pressing time remained highly significant. Py-GC/MS, FTIR spectroscopy and TGA indicated the formation of ester linkages with carbohydrate-derived OH-groups and the involvement of lignin moieties in the CA-ULHPB. This research identified optimal panel compositions and processing parameters for fabricating environmentally friendly composite panels using CA as a natural adhesive and hemp hurd as an agricultural by-product. The panels exhibited excellent properties and would be well suited as core layers in lightweight sandwich composites given their ultra-low-density range.

1. Introduction

The United Nations has estimated that the global population will increase by 21.3% to reach 9.7 billion by 2050 (UN, 2022). Concurrently, urbanisation is expected to rise to 68% in the same year, representing a 23.6% increase from 55% in 2018 (UN, 2018). Meeting the demands of the expected surge in residential and commercial development poses significant challenges for both manufacturers and consumers in terms of securing adequate and sustainable raw materials to produce the necessary building components. Particulate wood-based panels (PWBPs) are well-established building materials and extensively used in mass furniture manufacturing and as constituents for functional and decorative building products e.g., internal partitioning, wall, or ceiling linings. Common PWBPs include particleboard (PB), medium- and high-density fibreboard (MDF; HDF), oriented strand board (OSB) and various fibreboard materials. The combined global particle/fibreboard production is expected to grow by 72% to 593 million m^3 in 2050 (FAO, 2022). As competition for dwindling resources intensifies and supply chains are more frequently disrupted, manufacturers are increasingly forced to accept raw materials with greater inconsistencies, often from further distances and at higher costs (Sam-Brew and Smith, 2017). Additionally, most engineered wood products (EWPs) contain synthetic, petrochemical-based resins that may emit formaldehyde and VOCs during production and in-situ, thereby raising persistent concerns regarding their potential impact on human health. While fossil fuel-based binders have proven very effective in PWBPs and EWPs, their use also presents significant environmental challenges with respect to their origins, recyclability, and disposal of the materials with which they

* Correspondence to: The Sustainable and Renewable Forest Products Group, School of Agriculture, Food and Ecosystem Sciences (SAFES), Faculty of Science, The University of Melbourne, 500 Yarra Boulevard, Richmond 3121, Australia.
E-mail address: jfehrmann@unimelb.edu.au (J. Fehrmann).

https://doi.org/10.1016/j.indcrop.2024.118070
Received 14 September 2023; Received in revised form 7 December 2023; Accepted 8 January 2024
Available online 28 January 2024

are integrated. Together, these challenges motivate research efforts to lower formaldehyde emissions (Mert et al., 2022; Vineeth et al., 2019) and reduce the reliance on fossil resources (Mert et al., 2023) in current urea formaldehyde adhesives used in many EWPs. Simultaneously, there is a focus on developing building materials, either made entirely from or incorporating alternative renewable lignocellulosic raw materials, such as horticultural or agricultural by-products, along with '*biobased*' binders. Narrowly defined, '*biobased*' refers to natural substances of non-mineral origin i.e., tannins, lignins, carbohydrates, proteins and protein hydrolysates, dissolved wood, and auto adhesion (Pizzi et al., 2020).

Industrial hemp (*Cannabis sativa* L.) is one of the examined by-products for sustainable PB (Sam-Brew and Smith, 2017; Fehrmann et al., 2022, 2023a; Kirilovs et al., 2021; Zvirgzds et al., 2022; Alao et al., 2020). Hemp is a fast growing dioecious annual plant with a rich global history of cultivation for its fibre, seed, and, more recently, industrial cannabidiol extraction. The European Environmental Agency recognised hemp's superiority in a ranking of environmental indicators like nutrition depletion, pesticide needs, soil compaction, and agro-biodiversity (Petersen et al., 2007). In late 2017, a change in the Australia New Zealand Food Standards Code legalised hemp seed production for human consumption, leading to a resurgence of hemp cultivation in Australia. As of 2021/22, the estimated national production area is 2500 ha, with a shift towards biomass production over grain (Gordon and Miao, 2022). The residual xylemic inner part of the hemp stalk (*hurd*) is commonly regarded as a by-product after the removal of the grain and/or bast fibres. It is a porous, lightweight material with an apparent density between 88 - 133 kg/m^3 (Delhomme et al., 2020; Viel et al., 2018). The low raw material density and short fibre lengths ensure sufficient particle contact for low-density cores in sandwich biocomposites. Unlike general-purpose PB or fibreboard, sandwich panels are designed for specific functionalities and are comprised of a lightweight core sandwiched between face laminates. For the rapidly growing flat-pack furniture industry and the building sector, these engineered lightweight panels offer e.g., superior strength-to-weight ratios, improved raw material efficiency and design flexibility, and better ease of handling (Khojasteh-Khosro et al., 2020; Burnett and Kharazipour, 2017). Beyond cabinetry, there is potential to enhance the capabilities of hemp-core sandwich panels for various applications, spanning from non-load-bearing wall partitions to cladding and ceiling tiles. These panels could serve aesthetic or acoustic functions within residential or commercial prefabricated modular construction systems. Moreover, they might be explored as a building component to provide temporary shelter during fire or flood emergencies, particularly when outfitted with appropriate laminates for reinforcement.

Furthermore, hemp hurd's chemical composition is similar to that of timber, (Schwarzova et al., 2017; Stevulova et al., 2014) indicating compatibility with citric acid (CA) for the fabrication of biobased, lightweight hemp particleboard. CA is a tricarboxylic acid that occurs naturally in citrus fruits and is widely used in various industrial and consumer applications. It is a key ingredient in products such as pharmaceuticals and cosmetics, serving as a pH stabiliser and flavouring agent, (Lee et al., 2020) plasticiser and bio-degradable food packing (Apelblat, 2014). Polycarboxylic acids (PCA) such as CA and 1,2,3,4-butanetetracarboxylic acid (BTCA) have equally exhibited potential as crosslinking agents in cotton cellulose textiles (Schramm and Rinderer, 1999) and shown to improve tensile strengths in CA-modified fir (*Abies alba* Mill.) and beech (*Fagus sylvatica* L.) wood (Vukusic et al., 2006).

Umemura et al. (2012) first investigated CA as the primary bonding agent in natural wood adhesive. Using Fourier-transform infrared (FTIR) analysis, they suggested that crosslinking-esterification occurred as chemical bonds formed between carboxyl and OH groups in CA-resinated bark mouldings (*Acacia mangium* Willd.). With densities ranging from 900 - 1300 kg/m^3, they reported specific MOR and MOE values of 18.1 MPa and 4.9 GPa, respectively, for 20 wt% CA specimen pressed at 180 °C and 4 MPa for 10 min

Subsequently, numerous studies (Wibowo et al., 2021; Kusumah et al., 2017, 2016; Liao et al., 2016; Umemura et al., 2013, 2015; Ferrandez-Garcia et al., 2020; Santoso et al., 2020; Sutiawan et al., 2021; Sun et al., 2019) investigated the effect of CA on e.g., lignocellulosic raw materials (timber, vegetal by-products), product types (lamellas, veneer, and particulate panels), additional reactants for treatment efficiency (glycerol, glucose, sorbitol), and processing parameters (CA and reactant content, pressing temperature, moisture content). In a recent literature review on CA-bonded PB, (Lee et al., 2020) the favourable essential processing parameters were summarised as: i) CA content ranging from 20 to 30 wt%, ii) pressing temperature between 180 to 200 °C for 10 min, iii) panel density of 800 kg/m^3 , and iv) pre-drying treatment lasting 12 h at 80 °C.

Earlier mentioned research of CA and textiles, in wood modification, and more recently, CA combined with polyols (sorbitol), (Kurkowiak et al., 2022) suggested a reaction mechanism that involved the dehydration of the CA OH group, resulting in the creation of a cyclic anhydride. This anhydride is thought to subsequently establish ester connections with carbohydrate OH groups through nucleophilic substitution, as illustrated in Fig. 1a. While the possibility of an anhydride intermediate exists, it is important to note that the processing parameters in these studies may not align with the favourable conditions for CA-bonded PB, as previously summarised.

Research on the chemical bonding structures of Japanese cedar powder (*Cryptomeria japonica* (L.f.) D. Don) when blended with 20 wt% CA and subjected to hot pressing at 180 °C for 10 min, proposed a more direct reaction mechanism via the Fischer esterification pathway (Ando and Umemura, 2021). The same study also documented the esterification of diverse wood constituents, encompassing polysaccharides and lignin substructures (Fig. 1b). Nonetheless, besides reporting ester bonds with polysaccharides in poplar wood veneers (*Populus sp.)*, Del Menezzi et al. (2018) were the first to demonstrate CA esterification with various aromatic and aliphatic lignin components, as shown in Fig. 1c and d.

A lack of research on residual biomass and agricultural by-products as the primary raw material for low-density particleboard (<500 kg/m^3) has resulted in a focus on fossil fuel-based binders and synthetic resins. Natural binders such as CA have the potential to produce sustainable and biobased PB from hemp, yet this area remains significantly underinvestigated. This study examined how variations in composition (particle size and CA content) and pressing parameters (temperature and time) affected panel expansion (springback), internal bond strength (IB), water absorption (WA), and thickness swelling (TS) of CA-bonded ultra-low-density hemp PB (CA-ULHPB). Chemical compounds, thermal stability properties, and functional group presence were analysed both in the unmodified hurd and the CA-ULHPB using pyrolysis-gas chromatography-mass spectrometry (Py-GC/MS), thermogravimetric analysis (TGA), and Fourier-transform infrared (FTIR) spectroscopy, respectively.

2. Experimental

2.1. Materials

Decorticated hemp hurd chips (*Cannabis sativa* L.) of the dual purpose variety 'Frog1′ were sourced from the Gippsland region in Victoria, Australia. The chips were cleaned under running tap water, dried at 60 °C for 4 h and then conditioned at 23 °C and 65% relative humidity (RH) until constant mass was achieved (EMC). All subsequent processing steps involved hemp hurd conditioned to EMC. Anhydrous citric acid (C0759) was purchased from Sigma-Aldrich (Macquarie Park, Australia). A 59% concentrated CA solution was prepared by dissolving CA in demineralised water at a 59:100 ratio.

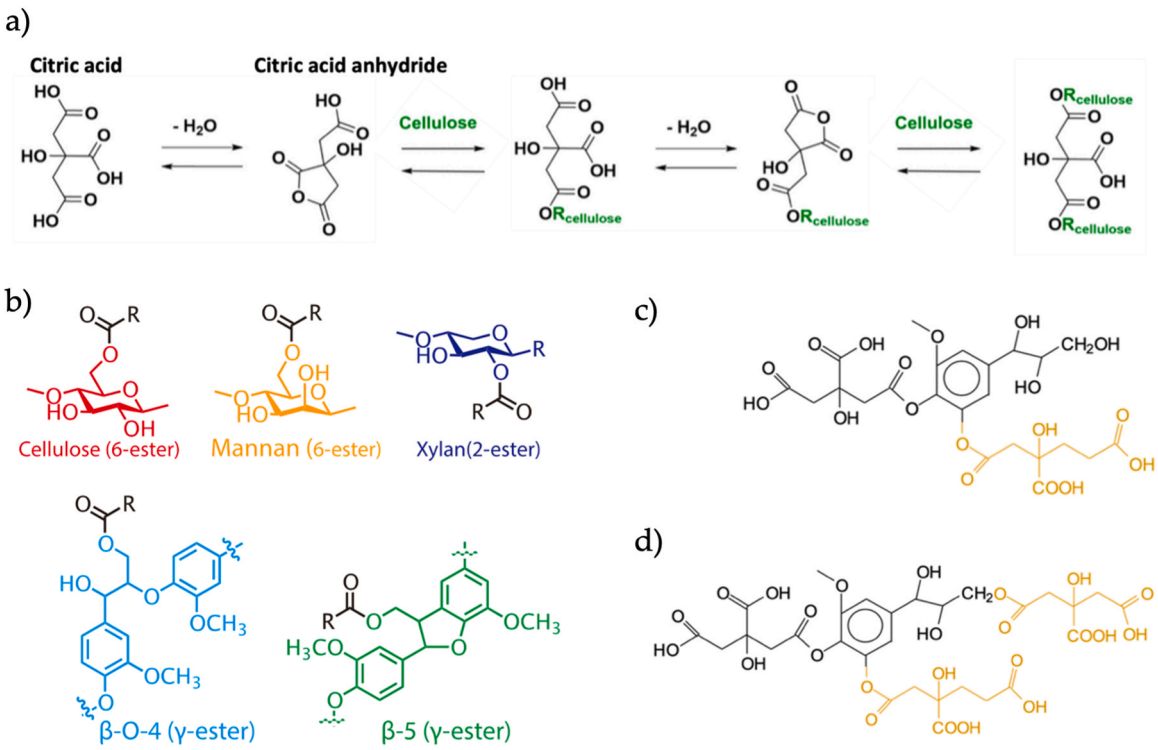

Fig. 1. Esterification pathways and structures.
(a) Citric acid dehydration to cyclic anhydride and subsequent formation of ester linkages with cellulose (adapted) (Kurkowiak et al., 2022). (b) Esterification of wood components after hot-pressing (adapted) (Ando and Umemura, 2021). Proof of lignin unit alcohol side chain -OH reaction with citric acid showing (c) peak at 613.8 Da and (d) peak at 789.4 Da (adapted) (Del Menezzi et al., 2018).

2.2. Methods

2.2.1. Panel fabrication

Hemp hurd chips were comminuted using a cutting mill (Fritsch Pulverisette 15, Germany) with a 6 mm perforated insert. The resulting furnish was then sieved through mesh apertures of 4.0, 2.0, 1.0 and 0.6 mm. Three particle size classes (PSCs) were produced by excluding particles that were retained on the 4.0 mm mesh (oversize) and those passing the 0.6 mesh (undersize). These included coarse (C: 2.0 – 4.0 mm), medium (M: 1.0 – 2.0 mm), and fine (F: 0.6 – 1.0 mm) particle sizes.

Particle dimensions and shape characteristics for each PSC were assessed using a methodology outlined by Picandet (Picandet, 2013) and described in earlier research (Fehrmann et al., 2022, 2023a).

In these studies, PSC-F had an adverse effect on synthetic binder-based ULHPB performance and was consequently omitted from the investigation involving CA. The CA-ULHPB therefore comprised the following particle size mixes (PSM): 1) 100% coarse particles homogeneously mixed (C), 2) a mixture of 50% coarse and 50% medium particles (CM), and 3) 100% medium particles homogeneously mixed (M). The premeasured particles for each panel variant were resinated in a sealed vessel with atomised CA solution (2.8 mm nozzle spray gun) at 30 wt% and 20 wt%, respectively, based on the particles mass conditioned to EMC. The CA-coated furnish was dried at 75 °C for 6 h followed by conditioning to EMC at 23 °C and 65% RH. Hand-formed single-layer mats were cast in an aluminium mould measuring 285 × 208×12 mm^3 and pre-compacted without heat at 0.42 MPa for 60 s. Thermocouple trials were conducted prior to the scale-up fabrication to assess the heat transfer profile within the mat. Following the removal of the casting frame, an aluminium caul plate was introduced, and the panels were pressed for 8 min and 12 min, referred to as *short* and *long* times, respectively, at a target pressure of 1.41 MPa. As a result, the CA-ULHPB exhibited densities ranging from 320 to 338 kg/m^3. The CA-ULHPB fabrication parameters are presented in Table 1.

2.2.2. Chemical and thermal properties

2.2.2.1. Pyrolysis-gas chromatography-mass spectrometry (Py-GC/MS). For the Py-GC/MS analysis, approximately 500 µg per sample were examined. The samples were placed in an eco-cup SF PY1-EC50F, covered with glass wool, and then subjected to pyrolysis at 500 °C for 0.1 min using a multi-shot pyrolizer (EGA/PY-3030D). The pyrolizer was connected (interface temperature 280 °C) to a GC/MS system QP-2020 NX (Shimadzu, Japan) with an SH-Rxi-5Sil MS column (30 m × 0.25 mm, film thickness 0.25 µm) at a pressure of 20.0 kPa (15.9 mL/min, column flow 0.61 mL/min) using helium as a carrier gas, and an electron impact of 70 eV. The GC temperature profile included a hold for 1 min at 50 °C, followed by a temperature rise to 280 °C (5 °C/min) and a 13-min hold at 280 °C. The identification of the pyrolysis products was carried out by comparing their retention times and mass spectra data with NIST LIBRARY 2017.14 (National Institute of Standards and Technology, 2017).

2.2.2.2. Fourier-transform infrared (FTIR) spectroscopy. The FTIR analysis was conducted using a Spectrum two instrument (Perkin Elmer Inc., USA) with attenuated total reflection (ATR) mode and equipped with Spectrum software (Ver. 10.5.3, Perkin Elmer Inc., USA). Spectra were recorded from approximately 0.1 g sample placed on a diamond plate, with 16 scans in absorption mode at a resolution of 4.0 cm^{-1}, covering a wavelength range of 4000 to 400 cm^{-1}.

2.2.2.3. Thermogravimetric analysis (TGA). A thermogravimetric analyzer (TGA 4000, Perkin Elmer Inc., USA) was employed to assess the thermal properties and stability of the neat hemp hurd from various origins and processing modalities as well as CA-ULHPB. Samples of approximately 10 mg ± 0.1 mg were placed in a crucible pan and

Table 1
Citric acid-bonded ultra-low-density hemp hurd particleboard (CA-ULHPB) fabrication parameters.

Variant type	Panel configuration				Pressing parameters				
	PSM	PSM Notation	Particle loading (g)	Citric acid (wt%)	Time (min)	Core mean temp. (°C)	Platen temp. (°C)	Pre-compaction (MPa)	Target pressure (MPa)
C.20.8	100% coarse	C	235.18	20	8	178.5	200.0	0.42	1.41
C.20.12					12	194.0			
C.30.8				30	8	178.5			
C.30.12					12	194.0			
CM.20.8	50% coarse + 50% medium	CM	235.60	20	8	178.5			
CM.20.12					12	194.0			
CM.30.8				30	8	178.5			
CM.30.12					12	194.0			
M.20.8	100% medium	M	235.39	20	8	178.5			
M.20.12					12	194.0			
M.30.8				30	8	178.5			
M.30.12					12	194.0			

PSM = Particle size mix

subjected to heating at a rate of 10 °C/min from 25 °C to 500 °C. During the analysis, a flow of nitrogen gas at 20 mL/min was maintained to prevent oxidation. Pyris software (Ver. 11.1.1, Perkin Elmer Inc., USA) was used to calculate the weight loss (TG) and differential thermogravimetry (DTG) of each sample.

2.2.3. Test preparation and assessment

After demoulding and cooling to room temperature, 8 thickness measurements were taken 25 mm away from the panel edges. The CA-ULHPB were subsequently conditioned to constant mass at 23 °C and 65% RH, and additional thickness measurements were taken before machining the specimens to evaluate panel springback. Springback is the moisture-dependent, permanent expansion in thickness of a compressed mat that occurs when compression stresses are relieved during hot-pressing (Kelly, 1977; Palardy et al., 1989). Excessive springback may result in debonding of the fibre-adhesive interphase and decrease mechanical strength properties (Mohebby et al., 2009). To evaluate the quality of particle bonding and dimensional stability properties of CA-ULHPB, specimens for internal bond strength (IB), water absorption (WA), and thickness swelling (TS) were prepared and tested following the guidelines of AS/NZS 4622.1 (AS/NZS, 4266.1, 2017). The obtained results were subsequently compared to the performance requirements outlined in AS/NZS 1859.1 (AS/NZS, 1859.1, 2017). Fig. 2a depicts surface details of CA-ULHPB manufactured from PSM-C, -CM and -M, respectively, while the schematic specimen cutting pattern is presented in Fig. 2b.

2.2.4. Data analysis and standard compliance

An analysis of variance test (ANOVA) was conducted using Minitab (Version 19.2020.2.0) at a significance level of $\alpha < 0.05$. The impact of particle size mix, CA content, and pressing time on IB, WA, and TS was assessed using a linear mixed model and Fisher's LSD comparison tests. The TS data was log transformed to meet the assumption of the error term. Compliance with AS/NZS 1859.1 (AS/NZS, 1859.1, 2017) involved comparing the 5-percentile IB and upper 95- percentile TS results with the lower ($L_{5\%}$) and upper ($U_{95\%}$) specification limit, respectively, set in the standards. $L_{5\%}$ and $U_{95\%}$ values were obtained by using Eq. 1 and Eq. 2 with untransformed data, respectively.

$$L_{5\%} = \bar{x} - ks_{\bar{x}} \quad (1)$$

$$U_{95\%} = \bar{x} + ks_{\bar{x}} \quad (2)$$

where $L_{5\%}$ is the lower 5-percentile comparison value of the sample (MPa), $U_{95\%}$ is the upper 95-percentile value of the sample (MPa), $\bar{x}$ is the grand mean (MPa), k is the factor used in the calculation of $L_{5\%}$ and $U_{95\%}$values, respectively (AS/NZS 4266.1 (AS/NZS, 4266.1, 2017) Appendix A; Table A1; k = 2.195), $s_{\bar{x}}$ is the estimate of the standard deviation between panel means.

3. Results and Discussion

3.1. Influence of composition on CA-ULHPB properties

3.1.1. Chemical and thermal properties

3.1.1.1. Pyrolysis-gas chromatography-mass spectrometry (Py-GC/MS). Py-GC/MS was employed as a screening method to identify and compare chemical compounds in untreated Frog1 hurd, CA-resinated Frog1

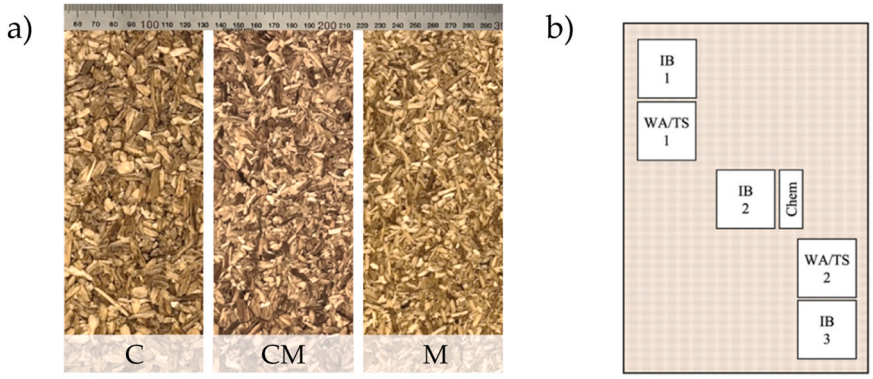

Fig. 2. CA-ULHPB surface detail: 100% coarse (C), 50% coarse and 50% medium (CM), 100% medium (M) (a) and schematic cutting pattern: IB = Internal bond strength, WA = Water absorption and TS = Thickness swelling, Chem = Py-GC/MS, FTIR, and TGA (b).

(dried but not hot-pressed), and CA-ULHPB. The Py-GC/MS chromatograms of the CA-ULHPB are shown in Fig. 3 and the identification and relative abundance of the principal pyrolysis products are presented in Table 2. Consistent characteristics observed in the pyrograms across all samples suggested that the fabrication parameters and constituent proportions had no significant effect on the chemical compounds present in CA-ULHPB. The dominant pyrolysis product (18″/19″) was identified as citraconic/itaconic anhydride, which originated from the dehydration and decarboxylation processes of CA (Wyrzykowski et al., 2010). All CA-ULHPB contained high levels of lignin moieties and primarily released compounds with syringyl (S) structures (red), while producing fewer guaiacyl (G)-units (blue). The main S-unit derivatives identified were syringol (55″), 4-methylsyringol (59″), 4-vinylsyringol (65″), trans-4-propenylsyringol (74″), syringylacetone (77″), and sinapyl alcohol (trans) (81″). The most prominent G-unit derivatives were guaiacol (35″), 4-methylguaiacol (46″), 4-vinylguaiacol (54″), and isoeugenol (trans) (60″).

Despite minimal differences in chemical composition among the CA-ULHPB samples, a comparison with the pyrogram of the raw material (raw Frog1 and CA-resinated Frog1) revealed substantial alterations during the formation of CA-bonded panels (exemplified by CM.30.12), as illustrated in Fig. 4. The pyrogram was divided into 3 regions, aligning with the sequential breakdown of easily decomposable carbohydrates (< 15 min), subsequent decomposition of lignin derivatives and phenolic components (>15 – 35 min), and extractives and fatty acids from 35 min onwards (Belleville et al., 2018).

Besides the major pyrolysis product citraconic/itaconic anhydride (3-methylfuran-2,5-dione), which implied the involvement of CA in the curing reaction, CA-ULHPB also exhibited furan compounds characterised by a single substituent group such as furfural and 3-methyl-2,4 (3 H,5 H)-Furandione. Previous research on sucrose/CA-bonded plywood (Zhao et al., 2019) suggested that the formation of furfural was attributed to the catalytic effect of CA on the dissolution of sucrose in during the heating process. The addition of sucrose to CA is believed to significantly improve the crosslinking reactions in lignocellulosic composites, primarily through the involvement of 5-hydroxymethylfurfural (5-HMF). This highly reactive furan derivative is generated during the thermal dissolution of sucrose. The formation of CA-ULHPB did not involve the intentional addition of sucrose and 5-HMF was not identified as a pyrolysis product. However, 5-HMF and furfural are the initial main products of saccharide pyrolysis and dehydration in biomass (Zhao et al., 2019; Hu et al., 2012) and have previously been discovered in hemp hurd but not in the leaves or roots of the plant (Salami et al., 2021). An increasing relative abundance of furfural is therefore considered as evidence of a reaction with CA (Zhao et al., 2019; Sutiawan et al., 2022).

During the same time frame, notable transformations occurred in the composition of CA-ULHPB, resulting in either complete decomposition or significant reduction of various compounds including 2-butanone (7), 2-Propanone, 1-(acetyloxy)- (8), 4-cyclopentene-1,3-dione (10), 2(5 H)-furanone (12), 6-Oxa-bicyclo[3.1.0]hexan-3-one (15), DL-threonine, N-glycyl- (24), cyclopropyl carbinol (34), and 2,4(3 H,5 H)-Furandione, 3-methyl- (37). Additionally, new compounds were identified during this process, namely 1,2-cyclopentanedione (17′), 2-methyliminoperhydro-1,3-oxazine (28′), and 3-cyclobutene-1,2-dione, 3,4-dihydroxy- (29′).

The subsequent phase was primarily characterised by the disappearance of lignin derivatives, including 1,2-Benzenediol, 3-methoxy- (46), acetoguaiacone (59), benzene, 1,2,3-trimethoxy-5-methyl- (60), coniferyl alcohol (75), sinapyl alcohol (cis) (78), catechol (41), and 1,3-Di-O-acetyl-.alpha.–.beta.-d-ribopyranose (56), a ribose derivative. The reduction of creosol (40) and 4-ethylguaiacol (47) was less pronounced, while guaiacyl acetone (62), syringaldehyde (71), and furan derivative 2,3-dihydrobenzofuran (42) exhibited a significant abundance decline. A newly formed compound, 4-ethylsyringol (62′′), was identified. Considerable increases in relative abundance were observed for 4-vinylsyringol (64) and syringylacetone (76), along with further rises of 4-

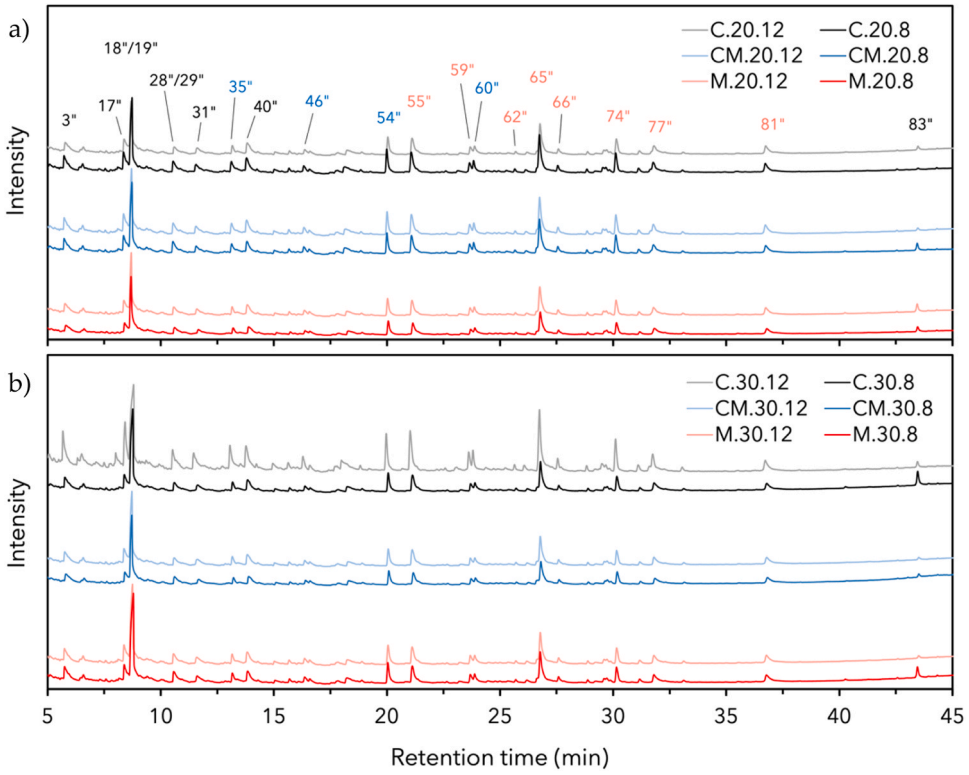

Fig. 3. Comparison by superposition of abridged Py-GC/MS chromatograms of CA-ULHPB fabricated with 20 wt% (a) and 30 wt% (b). Peak colours indicate compound origins: black = carbohydrate/protein, blue = guaiacyl-lignin, red = syringyl-lignin. C = 100% coarse, CM = 50% coarse and 50% medium, M = 100% medium, 20 and 30 = citric acid content (%), 8 and 12 = pressing time (min).

Table 2
Peak assignments and relative abundance of principal raw hurd and CA-ULHPB compounds released after Py-GC/MS.

Frog1		CA-ULHPB		Pyrolysis product	Origin	Relative abundance (%)													
Peak	Retention (min)	Peak	Retention (min)			Frog1 raw	Frog1 + CA	C.30.12	CM.30.12	M.30.12	C.30.8	CM.30.8	M.30.8	C.20.12	CM.20.12	M.20.12	C.20.8	CM.20.8	M.20.8
3	5.509	3"	5.677	Furfural	CH	2.95	3.87	4.16	5.24	5.03	n.d.	5.44	n.d.	4.84	4.57	n.d.	3.90	3.43	5.32
7	6.070	-	-	2-Butanone	CH	1.60	0.71	-	-	-	-	-	-	-	-	-	-	-	-
8	6.274	-	-	2-Propanone, 1-(acetyloxy)-	CH	1.07	0.66	-	-	-	-	-	-	-	-	-	-	-	-
10	6.710	-	-	4-Cyclopentene-1,3-dione	CH	0.93	0.50	-	-	-	-	-	-	-	-	-	-	-	-
12	7.674	-	-	2(5 H)-Furanone	CH	3.53	1.48	-	-	-	-	-	-	-	-	-	-	-	-
15	7.952	-	-	6-Oxa-bicyclo[3.1.0]hexan-3-one	E	5.68	4.29	-	-	-	-	-	-	-	-	-	-	-	-
-	-	17"	8.425	1,2-Cyclopentanedione	CH	-	-	6.23	5.17	6.33	4.01	4.57	4.42	4.85	5.85	5.38	5.99	5.14	n.d.
16	8.664	18"19"	8.6888.803	2,5-Furandione, 3-methyl- (Citraconic/ Itaconic anhydride)	CH	n.d.	34.95	18.42	19.91	22.32	22.79	21.70	25.39	15.84	14.57	18.30	17.41	16.69	20.47
24	10.168	-	-	DL-Threonine, N-glycyl-	N	2.52	3.29	-	-	-	-	-	-	-	-	-	-	-	-
-	-	28"	10.528	2-Methyliminoperhydro-1,3-oxazine	N	-	-	2.38	n.d.	2.79	n.d.	n.d.	n.d.	2.76	n.d.	n.d.	n.d.	n.d.	3.94
-	-	29"	10.550	3-Cyclobutene-1,2-dione, 3,4-dihydroxy-	CH	-	-	n.d.	2.91	n.d.	3.08	4.17	3.41	n.d.	3.49	2.98	3.43	n.d.	0.98
27	10.907	31"	11.461	1,2-Cyclopentanedione, 3-methyl-	CH	2.39	1.64	2.64	2.74	2.75	2.14	2.38	2.72	1.63	2.66	1.42	2.06	1.76	n.d.
33	12.816	35"	13.065	Guaiacol	G	2.61	1.63	4.02	2.35	1.73	2.05	2.01	2.03	1.84	2.05	1.72	2.01	1.77	1.75
34	13.123	40"	13.774	Cyclopropyl carbinol	E	4.28	2.39	4.22	5.41	3.69	4.79	4.83	4.19	5.52	4.80	4.13	4.71	4.16	4.30
37	14.036	-	-	2,4(3 H,5 H)-Furandione, 3-methyl-	CH	1.44	1.46	-	-	-	-	-	-	-	-	-	-	-	-
40	16.022	46"	16.290	Creosol	G	1.72	1.73	1.50	1.34	1.49	1.48	1.27	1.54	1.55	1.61	1.61	1.48	1.46	1.36
41	16.252	-	-	Catechol	E	2.57	1.30	-	-	-	-	-	-	-	-	-	-	-	-
42	16.872	-	-	2,3-dihydrobenzofuran	CH	4.39	3.46	-	-	-	-	-	-	-	-	-	-	-	-
46	18.107	-	-	1,2-Benzenediol, 3-methoxy-	G	1.81	1.22	-	-	-	-	-	-	-	-	-	-	-	-
47	18.587	-	-	4-ethylguaiacol	G	0.49	0.71	-	-	-	-	-	-	-	-	-	-	-	-
49	19.686	54"	19.973	4-vinylguaiacol	G	3.78	2.40	4.19	4.38	4.98	4.23	4.62	4.02	5.24	5.00	5.29	4.87	4.66	4.97
51	20.707	55"	21.030	Syringol	S	4.62	3.14	5.85	6.09	5.49	5.28	5.21	4.62	6.31	5.79	5.75	5.73	5.04	5.76
56	22.695	-	-	1,3-Di-O-acetyl-.alpha.-.beta.-d-ribopyranose	CH	1.85	0.30	-	-	-	-	-	-	-	-	-	-	-	-
57	23.318	59"	23.622	4-methylsyringol	S	n.d.	1.33	1.98	1.83	2.08	1.61	1.81	1.67	2.18	2.20	2.26	1.97	n.d.	1.70
58	23.525	-	-	Isoeugenol (trans)	G	1.75	0.88	2.09	2.44	2.15	2.52	2.60	2.20	2.48	2.48	2.72	2.43	2.45	2.72
59	24.472	-	-	Acetoguaiacone	G	0.52	n.d.	-	-	-	-	-	-	-	-	-	-	-	-
60	25.356	-	-	Benzene, 1,2,3-trimethoxy-5-methyl-	S	0.84	2.48	-	-	-	-	-	-	-	-	-	-	-	-
62	25.525	-	-	Guaiacyl acetone	G	1.82	2.23	-	-	-	-	-	-	-	-	-	-	-	-
-	-	62"	25.643	4-ethylsyringol	S	-	-	0.49	0.48	0.49	0.41	0.41	0.35	0.57	0.47	0.50	0.51	0.43	0.40
64	26.457	65"	26.746	4-vinylsyringol	S	6.43	3.06	8.07	9.83	9.14	9.64	8.86	9.65	10.62	13.37	10.44	12.72	13.02	9.54
67	27.303	66"	27.550	4-allylsyringol	S	0.80	0.44	1.04	1.02	1.05	1.04	1.08	1.58	1.22	1.76	1.20	1.66	2.07	1.05
71	28.774	-	-	Syringaldehyde	S	1.32	0.57	-	-	-	-	-	-	-	-	-	-	-	-
73	29.809	74"	30.108	4-propenylsyringol (trans)	S	3.14	1.40	3.88	3.64	3.90	3.24	3.86	2.85	4.53	4.34	4.50	4.49	4.37	3.95
75	30.767	-	-	Coniferyl alcohol	G	8.00	1.08	-	-	-	-	-	-	-	-	-	-	-	-
76	31.272	77"	31.751	Syringylacetone	S	1.13	0.87	2.59	3.52	3.00	3.33	3.27	2.66	5.04	3.96	3.68	3.83	3.93	3.32
78	34.557	-	-	Sinapyl alcohol (cis)	S	0.84	n.d.	-	-	-	-	-	-	-	-	-	-	-	-
79	35.510	-	-	Palmitic acid	CH	4.46	n.d.	-	-	-	-	-	-	-	-	-	-	-	-
80	36.220	-	-	Sinapyl alcohol (trans)	S	4.84	0.72	-	-	-	-	-	-	-	-	-	-	-	-
-	-	81"	36.729	Sinapaldehyde (trans)	S	-	-	1.96	2.64	2.79	2.11	2.60	2.04	3.12	2.98	3.05	2.55	2.44	2.49
82	39.222	-	-	Oleic Acid	CH	0.24	n.d.	-	-	-	-	-	-	-	-	-	-	-	-
83	39.509	-	-	Octadecanoic acid	CH	0.43	n.d.	-	-	-	-	-	-	-	-	-	-	-	-
-	-	83"	43.457	9-Octadecenamide, (*Z*)-	CH	-	-	0.56	0.53	n.d.	2.78	0.73	1.89	0.87	0.45	1.96	n.d.	1.47	1.40
84	48.191	-	-	(E)− 3,3′-Dimethoxy-4,4′-dihydroxystilbene	E	0.78	0.55	-	-	-	-	-	-	-	-	-	-	-	-

Origin: CH = carbohydrate; N = Protein; G = guaiacyl-lignin; S = syringyl-lignin; E = extractives, *n.d.* = not determined. C = 100% coarse, CM = 50% coarse and 50% medium, M = 100% medium, 20 and 30 = citric acid content (%), 8 and 12 = pressing time (min).

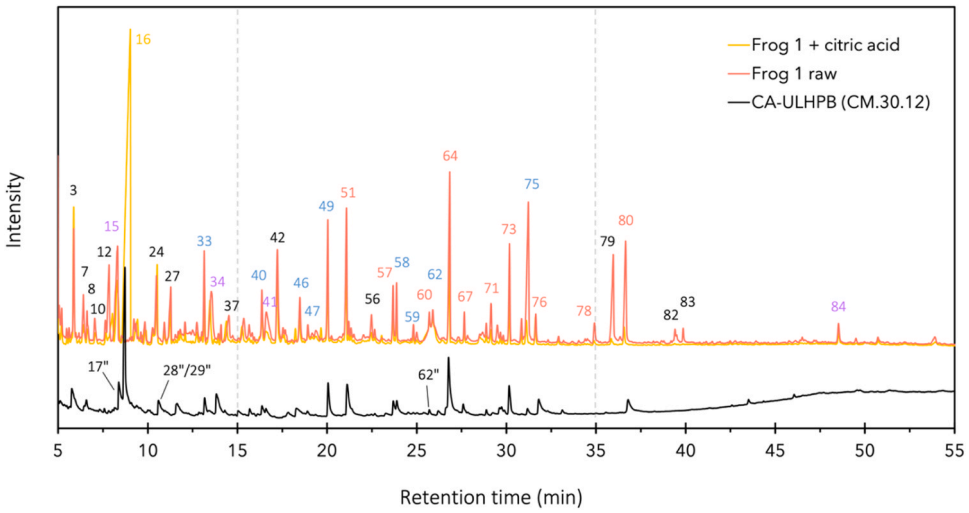

Fig. 4. Comparison by superposition of Frog1 and CA-ULHPB (CM.30.12) Py-GC/MS chromatograms. Colours of the peak numbers (Table 2) indicate compound origins: black = carbohydrate, blue = guaiacyl-lignin, red = syringyl-lignin, purple = extractives, yellow = citric acid.

vinylguaiacol (49), syringol (51), 4-methylsyringol (57), isoeugenol (trans) (58), 4-allylsyringol (67), and 4-propenylsyringol (trans) (73).

The last phase confirmed the absence of fatty acids, including palmitic acid (79), oleic acid (82), and octadecanoic acid (83). This lack may be ascribed to their reaction with the OH groups of the raw hemp, leading to the formation of covalent bonds that contributed to the adhesive mechanism (Belleville et al., 2018). Moreover, oxidative conversion of fatty acids promote the formation of carboxylic acids, (Randle et al., 1963) like CA, potentially increasing the bonding capacity in the panel via intrinsic generation in addition to the externally introduced CA. The phenolic compound (E)− 3,3‘-dimethoxy-4,4‘-dihydroxystilbene (84) disappeared as well, suggesting that the OH group participated in the reaction with CA.

The leading hypothesis explaining the adhesiveness of wood composites bonded with CA revolves around the formation of ester linkages between the carboxyl groups of CA and the OH groups present in wood components. These linkages facilitate crosslinking networks among the wood constituents, with a particular preference for readily accessible carbohydrate OH groups, especially those found in hemicelluloses. However, the Py-GC/MS analysis provided evidence of CA reactivity not only with carbohydrates but also with lignin, as evidenced by the substantial involvement of lignin moieties in the CA-ULHPB formation. Previous research (Del Menezzi et al., 2018; Amirou et al., 2017) provided strong support for the involvement of both aromatic and aliphatic OH groups of lignin in its reaction with CA, particularly the latter exhibiting alcohol-like behaviour. Moreover, the strong catalytic effect of CA was identified as the driving force behind internal rearrangements of lignin. This included the cleavage of CH_2OH groups, resulting in the formation of methanol, ethanol, and possibly propanol, along with reactions occurring on the aromatic carbons of lignin (ArC-H). Further observations revealed the cleavage of the bond between the aromatic ring and the alpha carbon of the aliphatic side chain, suggesting the formation of lignin derivatives that were significantly smaller in size than the original molecule. Importantly, these reactions were observed in 5-layer poplar plywood under conditions resembling the CA-ULHPB process (i.e., pressing at 180 °C for 20 min) (Del Menezzi et al., 2018). Furthermore, lignin condensation reactions have been documented within the temperature range of 165 °C to 180 °C, even in the absence of CA (Tjeerdsma et al., 1998). These reactions typically occur in the presence of hemicellulose cleavage products (depolymerisation) which subsequently engage in lignin polymerisation reactions (condensation), leading to increased lignin crosslinking amongst the composite constituents. Similarly, degradation products of carbohydrates may undergo additional transformations resulting in the formation of aromatic substances that contribute to the development of a pseudo-lignin macromolecule. The significance of pseudo-lignin in relation to CA-ULHPB will be explained in the upcoming section.

3.1.1.2. Fourier-transform infrared (FTIR) spectroscopy. FTIR spectroscopy was applied to qualitatively investigate the effect of CA content and pressing time in formed CA-ULHPB. Fig. 5 displays the FTIR spectra of raw Frog1 hurd in comparison with CA-ULHPB, organised by composition and pressing time. The absorption bands observed in the CA-ULHPB variants were comparable to those in the raw material, indicating that no modifications had occurred within the functional groups of the formed panels. Nevertheless, band intensities increased and were accompanied by (minor) peak shifts in some CA-ULHPB variants.

Vibrations around 3200 - 3800 cm^{-1} are associated with hydrogen bonded OH groups of the structural lignocellulosic components in the hurd as well as OH groups from carboxylic acids (Nitu et al., 2022; Chen et al., 2023). A decrease in absorbance at this band is attributed to a reduction of free OH groups bound up in the esterification reaction with CA (Liao et al., 2016; Nitu et al., 2022; Chen et al., 2023). Peak intensities were initially low in raw hurd but clearly intensified in most CA-ULHPB. Panels with 30 wt% CA and shorter pressing time of 8 min showed a (slightly) lower absorption (more reacted OH) at this band compared to panels pressed for 12 min. Conversely, longer pressing times led to significantly higher IB strength at 30 wt% CA and irrespective of PSM (Fig. 8a). Extended exposure to heat (200 °C) may have caused exposure of OH groups due to hemicelluloses depolymerisation, (Li et al., 2023) especially on the outer panel surface, coinciding with simultaneous increased OH reactions within the panel. The trend was found to be opposite in panels containing 20 wt% CA, where the presence of OH groups decreased with increasing pressing time. This suggests that a higher number of OH groups may have participated in chemical reactions during the pressing process compared to panels with shorter pressing times. This observation is supported by the consistently greater IB strengths observed in 20 wt% CA panels with 12-min pressing times (Fig. 8a). All CA-ULHPB panels exhibited peak shifts from 3334 cm^{-1} towards higher wavenumbers, indicating a decrease in OH bonding (Liao et al., 2016). However, the extent of this shift varied with panel composition and pressing parameters. The 30 wt% CA panels with 12-min pressing time showed the lowest peak shifts, with C < CM < M, and were also found to be the strongest mechanically. In contrast, the effect of composition and pressing parameters on the remaining panels was inconclusive.

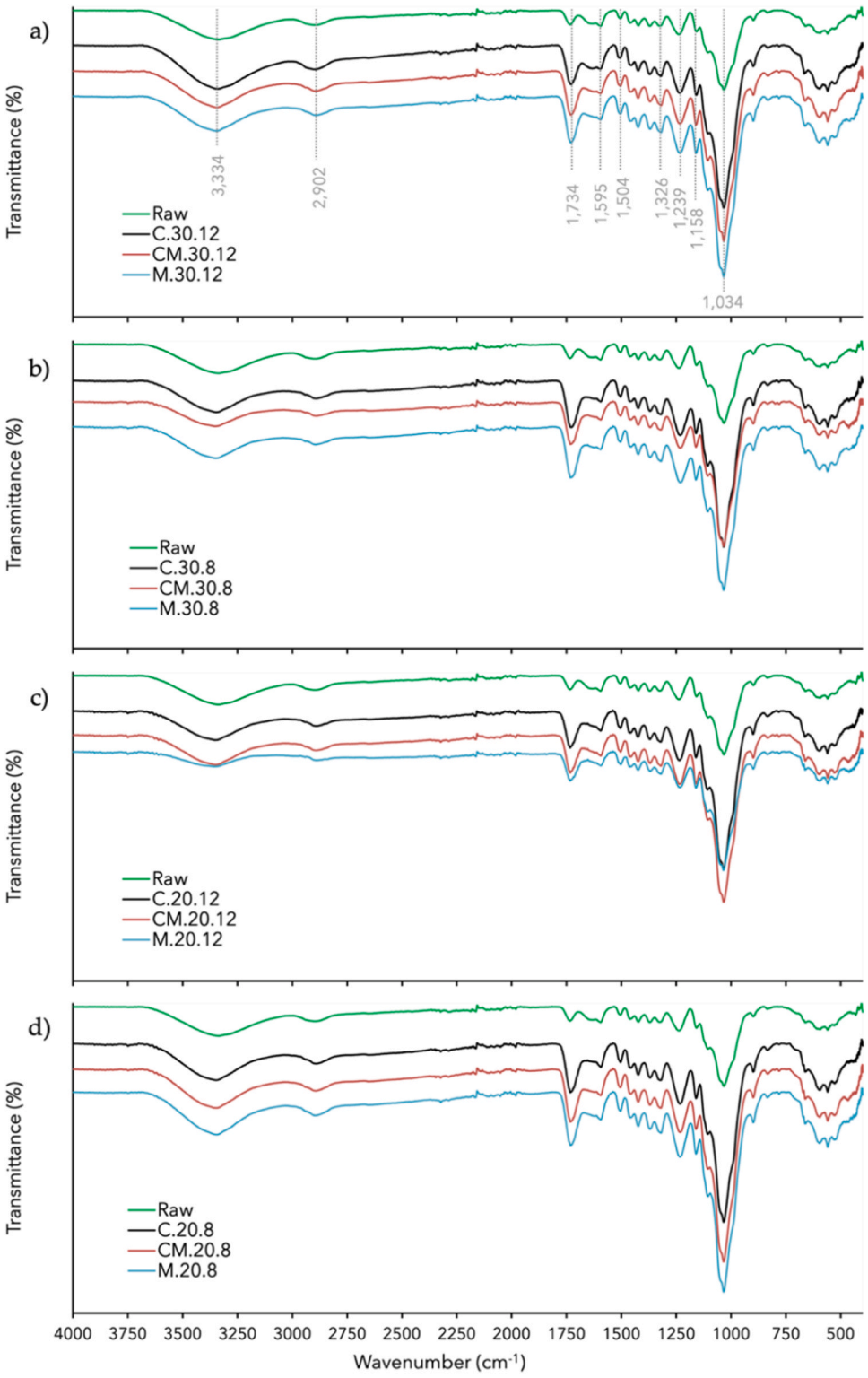

Fig. 5. FTIR spectra of raw Frog1 and CA-ULHPB. C= 100% coarse, CM = 50% coarse/50% medium, M = 100% medium. 30 and 20 = citric acid wt%; 12 and 8 = pressing time in min.

The 2800–3000 cm^{-1} range in the FTIR spectra indicated C-H stretching in the polymer network of the composite material, which included hemicelluloses, cellulose, and lignin in the hurd. Absorbance in this range increased uniformly in all panels, independent of PSM or fabrication parameters. A peak round 1734 cm^{-1} is considered as evidence of successful reactions between the raw material and CA (Umemura et al., 2012, 2015; Nitu et al., 2022). The band is believed to be intensified by C═O stretching, arising from the carbonyl group found in esters formed between CA and the OH groups of the hemp, and/or from the carboxyl groups of any remaining (unreacted) CA (Umemura et al., 2015). However, FTIR cannot selectively identify the ester groups, and it is only through procedures like boiling that residual CA is removed from the samples and bands can be obtained without interference from the carboxyl groups. Further treatment (boiling) of the samples was beyond

the scope of this study. Consequently, the absorbance around 1734 cm^{-1} was low in raw hurd and substantially increased in all CA-ULHPB. Although the 8-min variants exhibited greater absorption than their 12-min counterparts, no enhancement of IB strength was observed. This suggests that the greater 1734 cm^{-1} peaks at in PB with shorter pressing times may be caused by unreacted CA rather than greater esterification.

The absorption bands at 1595 cm^{-1} (C═C of aromatic ring), 1504 cm^{-1} (C═C of benzene ring), 1423 cm^{-1} (guaiacyl and syringyl condensed nuclei), 1326 cm^{-1} (syringyl C═O vibration) and 1239 cm^{-1} (guaiacyl C-O stretch) are indicative of lignin presence and significantly intensified in all CA-ULHPB. Chen et al. (2023) suggested that the greater peak intensities may be attributed to the formation of pseudo-lignin. Pseudo-lignin is a macromolecule that is believed to form during the hot-pressing process when carbohydrate hydrolysis products (e.g., furfural) repolymerise to form intermediate aromatic substances (Hu et al., 2012). These intermediates can then undergo further reactions, resulting in the formation of a three-dimensional structure with functional groups similar to native lignin. This process may have led to an increase in FTIR lignin signals in the resulting panels (Yang et al., 2015) and facilitated greater adhesion between particles. The peak intensities were not affected by CA content or prolonged pressing times, indicating that reactions already occurred at lower temperatures (178.5 °C mean core temperature in 8-min panels) and were exclusively related to the polymeric structure of the hurd. The peak intensity in all panels around 1158 cm^{-1} was greater than the raw hurd, suggesting the dehydration of OH groups (C-O-C formation) (Chen et al., 2023) and greater ester absorbances (C-O), (Halpern et al., 2014) which are both thought to improve auto adhesion in the panels. The 1034 cm^{-1} peak in the FTIR spectrum is a result of the C-O stretching of the carboxyl group found in CA which confirmed the involvement of CA in the esterification of hemicelluloses and cellulose (Nitu et al., 2022). Based on the FTIR spectra of sucrose and CA adhesive, Sun et al. (2019) suggested that additional bonding may occur in this absorbance range through ether linkages (C-O-R) formed by dehydration condensation of furan compounds.

3.1.1.3. Thermogravimetric analysis (TGA). TGA was utilised to investigate the thermal deterioration of both the raw Frog1 hurd and the formed CA-ULHPB. Fig. 6 displays the thermogravimetric (TG in wt%) and differential TG (DTG in mg/min) profiles of the CA-ULHPB alongside the original Frog1 raw material. Comprehensive thermal stability information is provided in Table 3. The thermal decomposition of CA-ULHPB, as observed in Fig. 6, exhibited a bimodal degradation pattern, consistent with previous findings on raw Frog1 and additional hemp hurd samples (Fehrmann et al., 2023b). The CA-ULHPB profiles showed a high degree of similarity suggesting that the degradation characteristics were not significantly affected by variations in particle size mix, CA content, or pressing time. Due to the earlier thermal breakdown of CA (175 °C to 203 °C) (Wyrzykowski et al., 2010; Moldoveanu, 2019) which preceded the degradation of hemicellulose and cellulose in phase II (>200 °C to 340 °C), the thermal stability of CA-ULHPB was slightly lower compared to raw Frog1. An important distinction between the raw material and the CA-bonded composites was the sustained decomposition of raw Frog1, with the residual weight (10.5%) being less than half of most CA-ULHPB (Table 3). The substantially higher residual weight of CA-ULHPB, indicated the successful reaction between CA and the hurd. The notably lower residual weight of M.30.8 (15.0%) and M.20.8 (16.5%), respectively, may be attributed to localised variations within the specimens since neither C nor CM equivalents exhibited a comparable level of weight reduction.

3.1.2. Springback, thickness, and density

Fig. 7a-c depict ULHPB thickness after demoulding and post conditioning. Springback was positively correlated with PSM and was the highest in short pressing time (8 min) variants for each PSM. The minimum (2.4%), and maximum (4.2%) springback were recorded in M.30.12 and C.20.8, respectively. PSMs and variants with 30% CA content and 12-min pressing time were almost indistinguishable. Smaller particles mesh more effortlessly whilst larger particles require more pressure and must be crushed to achieve the target thickness. Bavaneghi et al. (2015) suggested that densification may impede heat transfer and water vapour permeability towards the core layer. Short pressing times may also lead to inadequate particle plasticisation and insufficient curing of the binder, resulting in a lack of permanent bonding between particles surfaces. This may explain the greater springback in panels with coarse particles and 8-minute pressing time and emphasises the importance of adequate heat transfer towards the PB core. Fig. 7d-f show the moisture content and CA-ULHPB density after conditioning to EMC. Variants with 12-min pressing times recorded averagely 7% MC irrespective of PSM. Higher MC was recorded in panels with shorter press time but only C.20.8 and C.30.8 exceeded 8% MC. CA-ULHPB densities ranged from 320 kg/m^3 (C.20.12) to 338 kg/m^3 (M.30.8) following C < CM < M. The higher densities in CA-ULHPB with shorter pressing times can be attributed to greater MC. Lower densities in CA-ULHPB with PSM-C particles were caused by the greater springback. Thickness variability (i.e., density) is a common occurrence both

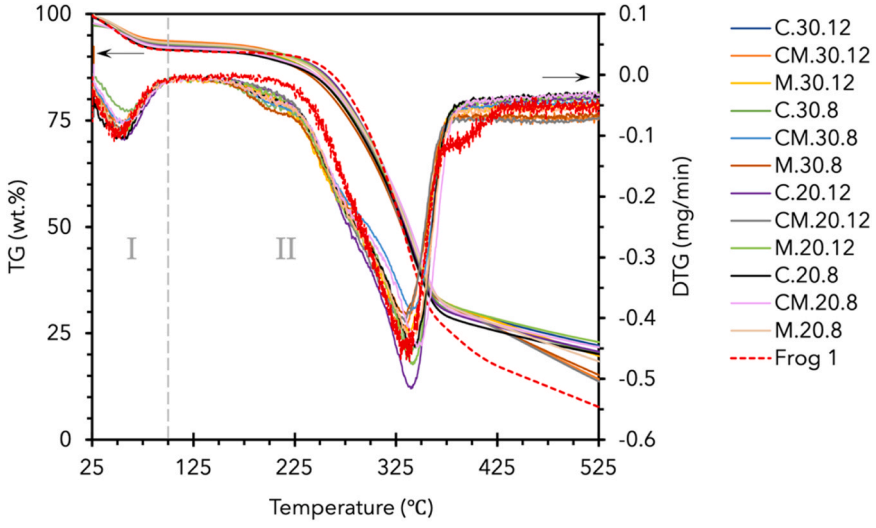

Fig. 6. Thermogravimetric (TG) and differential TG (DTG) profiles of CA-ULHPB and raw Frog1. C = 100% coarse, CM = 50% coarse and 50% medium, M = 100% medium, 20 and 30 = citric acid content (%), 8 and 12 = pressing time (min).

Table 3
Thermal stability details of CA-ULHPB and raw Frog1.

Phase	Variable	C.30.12	CM.30.12	M.30.12	C.30.8	CM.30.8	M.30.8	C.20.12	CM.20.12	M.20.12	C.20.8	CM.20.8	M.20.8	Frog1
I	Weight loss (%)	6.2	6.0	7.0	4.3	6.3	6.9	7.5	7.5	7.2	8.5	6.1	6.9	8.2
	DTG peak (°C)	54.6	56.6	53.4	60.7	56.0	56.1	56.0	53.2	53.5	58.8	61.6	51.9	46.7
II	Weight loss (%)	66.8	71.2	67.1	68.6	67.4	78.2	68.0	69.8	67.1	67.9	67.1	76.6	81.3
	DTG peak (°C)	341.6	329.0	338.2	339.9	340.8	334.9	339.6	334.0	341.3	340.0	345.2	337.9	338.3
Total weight loss (%)		73.0	77.2	74.1	73.0	73.6	85.0	75.5	77.2	74.3	76.3	73.2	83.5	89.5
Residual weight (%)		27.0	22.8	25.9	27.0	26.4	15.0	24.5	22.8	25.7	23.7	26.8	16.5	10.5
Weight loss at 100 °C (%)		6.7	6.3	7.1	6.7	6.9	6.9	7.4	7.1	6.9	8.4	7.8	6.7	8.5
T-5% (°C)		67.0	68.0	62.9	63.2	64.0	64.5	63.6	63.0	64.9	55.5	58.1	65.1	54.2
T-10% (°C)		220.6	220.5	208.7	206.7	207.5	201.3	222.6	220.7	221.7	192.0	199.3	215.9	227.1
T-20% (°C)		274.0	272.0	267.6	270.1	269.5	264.1	275.6	273.4	274.0	268.2	270.1	273.2	281.2
T-60% (°C)		350.4	347.2	348.9	349.1	354.1	347.6	348.0	347.4	351.2	347.6	353.5	351.6	343.5
T max (°C)		341.6	329.0	338.2	339.9	340.8	334.9	339.6	334.0	341.3	340.0	345.2	337.9	338.3

C = 100% coarse, CM = 50% coarse and 50% medium, M = 100% medium, 20 and 30 = citric acid content (%), 8 and 12 = pressing time (min).

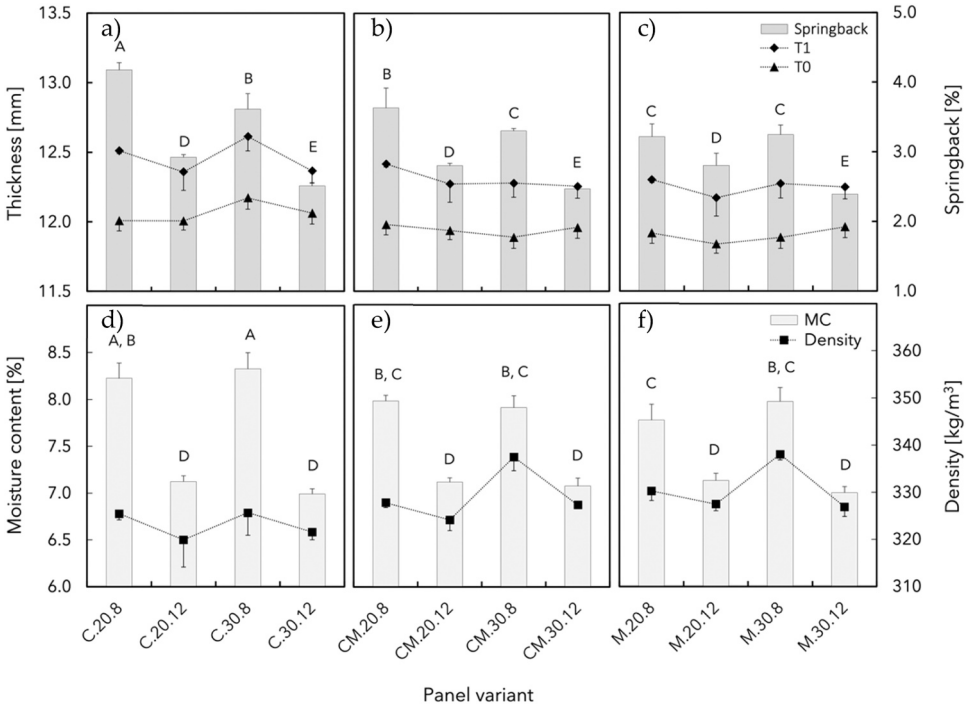

Fig. 7. Comparison between CA-ULHPB thickness and springback (a-c) and moisture content and density at EMC (d-f). T_0 and T_1 indicate panel thickness before and after conditioning, respectively. Error bars indicate standard deviations. Means that do not share a letter are significantly different. C = 100% coarse, CM = 50% coarse and 50% medium, M = 100% medium, 20 and 30 = citric acid content (%), 8 and 12 = pressing time (min).

within and between panels of hand-formed PB, as reported in previous studies (Sam-Brew and Smith, 2017; de Souza et al., 2014; de Melo et al., 2009).

3.2. Physico-mechanical properties of fabricated CA-ULHPB

3.2.1. Internal bond strength (IB)

Fig. 8a presents the comparison of IB, and Fig. 8b depicts the relationship between IB and springback. The range of IB values spanned from 0.09 MPa (C.20.8) to 0.19 MPa (C.30.12). The highest IB was achieved using 30% CA and a pressing time of 12 min. Pressing time did not significantly affect IB in CM and M variants with 20% CA but was significant in C.20.12. The influence of CA% and pressing time was only significant in PSM-C and decreased with decreasing particle size in PSM-CM and M. Despite lower densities, panels with larger particles (C) and a 12 min pressing time exhibited greater IB. The particle size analysis revealed that PSM-C had the most voluminous particles with short and thick shapes (least elongation). These characteristics have been linked to improved IB in some studies, (Fehrmann et al., 2022; Kawai and Sasaki, 1993; Sackey et al., 2008; Li et al., 2010) although other studies have reported higher IB in the presence of smaller particles (Maloney, 1977; Cosereanu et al., 2015; Nemli, 01/01, 2003). PSM-C comprised the most favourable particle dimensions and resulted in superior IB when pressed for 12 min. Longer pressing times ensured sufficient heat transfer into the CA-ULHPB cores and have previously been linked to greater IB in CA-bonded sweet sorghum bagasse PB pressed at 200 °C (Kusumah et al., 2017).

A positive correlation between IB and springback demonstrated that lower pressing times resulted in greater thickness expansion and lower IB. Despite experiencing less springback, variants with smaller particle sizes showed a more pronounced decrease in IB. This might be attributed to their larger specific surface area: PSM-CM and M had lower amounts of CA solution per unit area at equal particle loadings, leading to uneven binder distribution and weaker bonding. Typically, the strength properties of EWBP improve with higher resin content, albeit at a diminishing rate (Maloney, 1977; Ashori and Nourbakhsh, 2008; Dunky and Pizzi, 2002; Shmulsky and Jones, 2011).

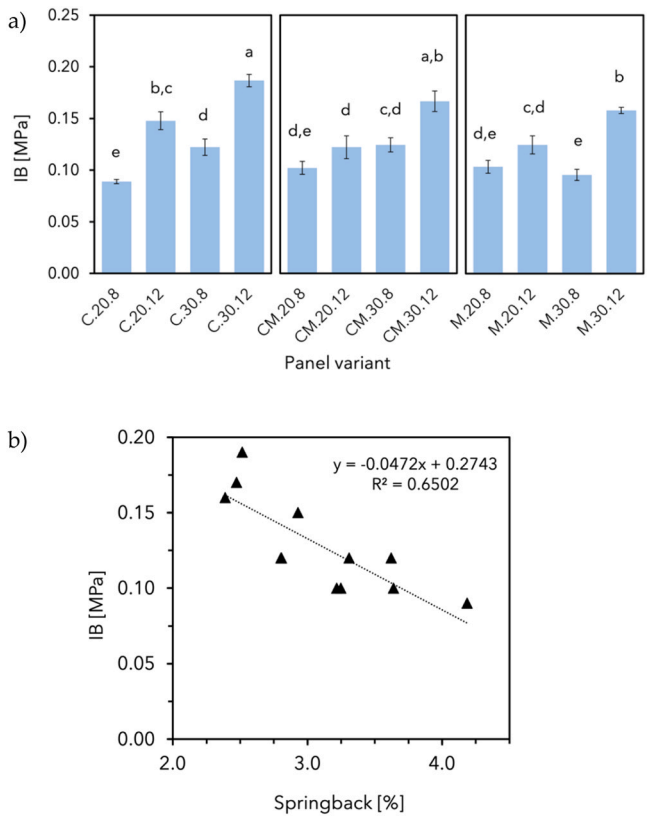

Fig. 8. Internal bond strengths (a) and relationship between IB and springback (b). C = 100% coarse, CM = 50% coarse and 50% medium, M = 100% medium, 20 and 30 = citric acid content (%), 8 and 12 = pressing time (min). Error bars indicate 95% CI. Means that do not share a letter are significantly different.

3.2.2. CA-ULHPB internal bond strength (IB) versus particleboard

A comparison of the IB strengths with the AS/NZS 1859.1 (AS/NZS, 1859.1, 2017) performance specifications required the calculation of the lower 5-percentile ($L_{5\%}$) values which are presented in Table 4. The $L_{5\%}$ for standard PB in the nominal thickness range of > 12–22 mm is 0.30 MPa. The CA-ULHPB minimum and maximum IB $L_{5\%}$ were 0.08 MPa (M.30.8) and 0.17 MPa (C.30.12), respectively. Consequently, none of the CA-ULHPB variants met the minimum IB threshold for standard PB (dry conditions). However, higher panel densities typically lead to improved strength properties, including IB, assuming adequate binder and appropriate curing. This is primarily facilitated by a greater amount of raw material available to withstand mechanical loads, as well as a greater particle contact, which allows for better utilisation of resin that would otherwise be lost in the interparticle voids. To achieve sufficient particle contact, compression ratios (CR) between 1.2 - 1.6 are generally considered adequate (Maloney, 1977; Suchsland, 1959). The CR of the CA-ULHPB was found to be 1.43, which falls within this range. It is worth noting that conventional Australian PB below 13 mm thickness exhibit notably higher panel densities, typically ranging from 660 to 700 kg/m^3 (EWPAA, 2008).

Table 4
CA-ULHPB compression ratios (CR) and internal bond strength (IB) 5-percentile comparison values.

Variant type	CR	IB		
		$\bar{x}$	$s_{\bar{x}}$	$L_{5\%}$
		(MPa)		
C.20.8	1.43	0.09	0.003	0.08
C.20.12		0.15	0.013	0.12
C.30.8		0.12	0.012	0.10
C.30.12		0.19	0.009	0.17
CM.20.8		0.10	0.010	0.08
CM.20.12		0.12	0.017	0.09
CM.30.8		0.12	0.010	0.10
CM.30.12		0.17	0.015	0.13
M.20.8		0.10	0.010	0.08
M.20.12		0.12	0.013	0.10
M.30.8		0.10	0.008	0.08
M.30.12		0.16	0.005	0.15

$\bar{x}$ is the arithmetic mean of all measurements obtained from a sample, $s_{\bar{x}}$ is the estimated standard deviation between panel means, $L_{5\%}$ is the lower 5-percentile comparison value of the sample, CRs were determined by dividing the panel density (unresinated furnish at EMC) with the raw material density (231 kg/m^3). The raw material density was established in a previous study (Fehrmann et al., 2022).

The American National Standards Institute (ANSI, 1999) further distinguishes three categories of PB densities: low (<640 kg/m^3), medium (640 to 800 kg/m^3), and high (>800 kg/m^3). With the CA-ULHPB density range reduced between 320 to 338 kg/m^3, the uniform structure consisting of a single layer, and adhesion primarily dependent on the presence of ester linkages between hurd particles, achieving a maximum IB strength of 0.17 MPa represents a promising outcome.

3.2.3. Water absorption (WA) and thickness swelling (TS)

Fig. 9a shows the WA and back transformed TS values following 2 h and 24 h of water immersion. In Fig. 9b, the relationship between springback, WA, and TS is presented after a 24 h duration.

The minimum and maximum WA after 2 h were 126% and 231% and recorded in C.30.12 and CM.20.8, respectively. Following 24 h, WA increased in both variants to a minimum and maximum of 183% and 269%, respectively. The data indicated that higher CA content and longer pressing time (treatment types) resulted in reduced WA after 2 h and 24 h, irrespective of PSM. However, only PSM-M exhibited statistically significant differences among all treatment types.

The impact of treatment effects diminished in each PSM as particle size increased except for the most distinct treatments (20.8 vs 30.12), suggesting that particle dimension had only minor effects on WA. The influence of water immersion on TS after 2 h and 24 h, respectively, followed a slightly different pattern compared to WA. The minimum and maximum TS values after 2 h were 9% (C.30.12) and 48% (C.20.8), respectively. After 24 h, the minimum and maximum TS values increased to 12% (CM.30.12) and 58% (C.20.8), respectively. Despite the consistent and significant impact of treatment types on TS within each PSM, there was a noticeable increase in TS with larger particle dimensions following C > CM > M, with the most prominent difference observed among the 20.8 variants. However, as the CA content and pressing time increased, this pattern weakened, and no statistically significant difference between equivalent CA-ULHPB variants remained suggesting that sufficient bonding amongst the particles had occurred irrespective of PSM. Differences between low contrast treatments (i.e., 20.12 vs 30.8) diminished in WA but were highly significant in TS across all PSMs.

These findings indicated that higher CA content alone cannot effectively reduce TS in the CA-ULHPB. Instead, the longer pressing time of 12 min proved to be the decisive factor in promoting stronger cross-linking among the particles. Acknowledging prior research, (Kusumah et al., 2016; Amirou et al., 2017) it is important to note that increased participation of CA, facilitated by heat and availability, may have contributed to enhanced water resistance. This is because CA is thought to react with the OH groups present in the lignocellulosic components.

Equally noteworthy is that despite a lower CA content of 20 wt%, the longer pressing time resulted in a significant decrease of 58.2% (C), 55.8% (CM), and 50.1% (M) in TS after 24 h, when comparing the 20.12 and 20.8 variants. This indicated that the 8-min pressing time was inadequate and may have resulted in incomplete curing of CA in the CA-ULHPB. However, the assessment of unreacted CA levels was not within

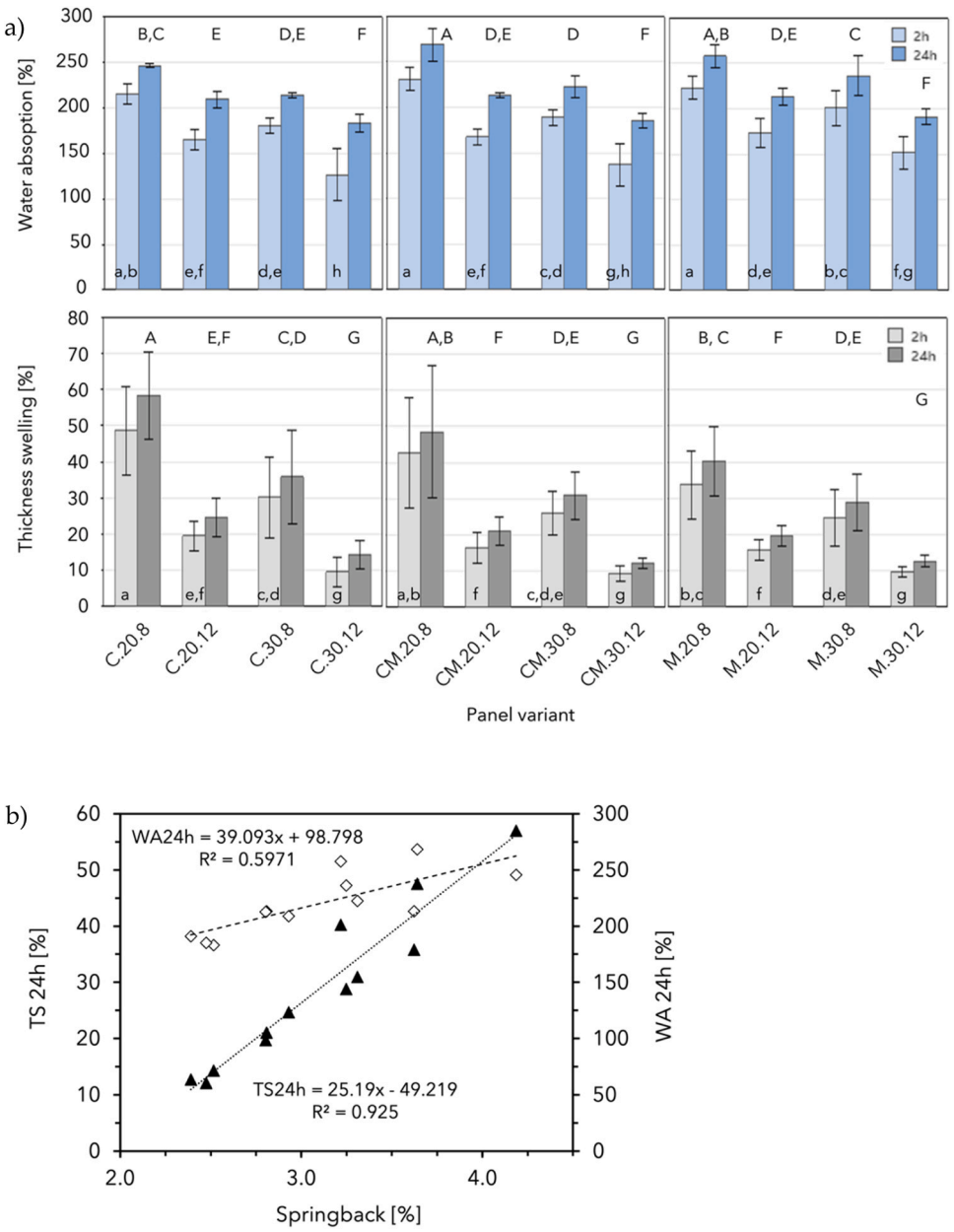

Fig. 9. Water absorption (WA) and back transformed thickness swelling (TS) after 2 h and 24 h, respectively (a) and relationship between springback and TS and WA after 24 h (b). Error bars indicate 95% CI. TS uses back transformed data. Means that do not share a letter are significantly different (2 h = lower case, 24 h = upper case). C = 100% coarse, CM = 50% coarse and 50% medium, M = 100% medium, 20 and 30 = citric acid content (%), 8 and 12 = pressing time (min).

the scope of this study. Nonetheless, techniques such as FTIR spectroscopy of samples subjected to cyclic aging protocols, including boiling, as well as the comparison of pH levels of residual water, could be utilised to determine the proportions of unreacted CA (Kusumah et al., 2017, 2016). The response of CA-ULHPB to water immersion followed similar patterns observed in previous studies that utilised CA alone for bonding lignocellulosic particles (Kusumah et al., 2017, 2016; Del Menezzi et al., 2018; Amirou et al., 2017; Syamani et al., 2018, 2020). These studies established that increasing the CA content and extending the pressing time led to improved dimensional stability of the panels up to a certain threshold. However, exceeding a 15-min pressing time at 200 °C and CA concentrations beyond 30 wt% seemed to have counterproductive effects. At these levels, the lignocellulose material might begin to degrade, and excessive CA could lead to brittleness, thereby adversely affecting the mechanical performance. The properties of New Giant Reed (*Arundo donax* L.) composites showed consistent improvements with higher CA contents when the panel densities were increased (Ferrandez-Garcia et al., 2019). This was attributed to the greater availability of particles per unit area in denser panels, enabling a larger number of OH groups from the particles to engage in the formation of ester linkages with the carboxyl groups of CA. As a result, stronger and more extensive crosslink networks were formed, leading to enhanced resistance against panel expansion. Conversely, panels with lower density contained less available material and larger voids, which enabled greater water ingress and swelling, and subsequently increased stress on the bonds.

As all CA-ULHPB were formed with similar particle loadings, the theoretical panel densities (mass of conditioned resinated particles divided by expected panel volume at 12 mm thickness) were primarily affected by differences in CA content. This resulted in a modest 3.5% density increase of the 30 wt% CA variants compared with the 20 wt% equivalents which does not suffice to explain the differences in dimensional stability among the CA-ULHPB. On the other hand, the springback

observed in WA 24 h and TS 24 h samples, indicating panel expansion with subsequent density loss, aligned well with the previously mentioned inverse correlation between density and WA and TS, as depicted in Fig. 9b.

3.2.4. CA-ULHPB dimensional stability versus moisture resistant particleboard

A comparison of the TS results after 24 h water immersion with the AS/NZS 1859.1 (AS/NZS, 1859.1, 2017) performance specifications required the calculation of the upper 95-percentile ($U_{95\%}$). $U_{95\%}$ values were computed from the raw TS 24 h means and depicted in Fig. 10.

The threshold for moisture resistant PB in the nominal thickness range of > 12 to 22 mm was 15.0%. CM.30.12 and M.30.12 attained $U_{95\%}$ values of 13.2% and 14.5%, respectively, and were the only variants that successfully fulfilled the upper specification limit for moisture-resistant PB. Conversely, all other variants, including PSM-C's C.30.12 with the lowest $U_{95\%}$ value of 18.4%, exceeded the 15.0% threshold. Previous research on wood and non-wood lignocellulosic raw materials (Marbun et al., 2023) demonstrated that thermal pre-treatment, specifically steaming, alleviated internal stresses stored in cellulose microfibrils. Assuming a similar effect, utilising pre-treated hurd could lead to a TS decrease in CA-ULHPB.

AS/NZS 2017 does not define performance specifications for WA. It is important to mention that CA-ULHPB were fabricated as uniform, single-layer mats, without deliberate surface compaction which can delay water ingress. Moreover, this study did not employ wax or additives, which are commonly used in the manufacturing of industrial particleboard to enhance dimensional stability.

3.3. CA-ULHPB overall observation

The use of 30 wt% CA combined with a 12-min pressing time yielded the most favourable IB and dimensional stability (WA and TS) characteristics in this study. In contrast, CA-ULHPB with an 8-min pressing time exhibited greater springback, regardless of the CA content, and seemed inadequate for effectively plasticising larger particles (PSM-C). This inadequacy had a detrimental impact on both the IB and dimensional stability of CA-ULHPB. On the other hand, the reduced MC in CA-ULHPB with the 12-min pressing time suggested greater moisture involvement during panel formation, enhancing particle plasticisation. The extended pressing time also allowed sufficient time for heat and water vapor to penetrate the mat core. This effectively mitigated the increased densification of the crushed larger particles and enabled more effective bonding between CA and lignocellulosic OH groups. However, the improved adhesion among particles experiencing higher temperatures (due to longer pressing times) cannot be solely attributed to the increased availability of CA per unit area. Elevated temperatures also played a significant role in promoting a higher level of OH group participation in the chemical reaction with CA, as evidenced by the FTIR peak intensities observed in CA-ULHPB, both in the 3200 - 3800 cm^{-1} range and around 1158 cm^{-1}.

The heightened involvement of OH groups, primarily originating from thermally less stable hemicellulose, likely contributed to the reduction of both WA and TS, in addition to the previously mentioned superior IB strength. Furthermore, Py-GC/MS analysis revealed potential contributions from fatty acids to interparticle adhesion, along with the involvement of lignin components in the bonding mechanisms of CA, and the possible participation of pseudo-lignin. The greater relative abundance of furfural in formed CA-ULHPB equally suggested greater crosslinking reactions with CA.

4. Conclusion

This study confirmed the feasibility of using citric acid (CA) to fabricate environmentally friendly ultra-low-density hemp hurd particleboard (ULHPB) with densities ranging from 320 to 338 kg/m^3 . The research demonstrated the ability to create single-layer CA-ULHPB variants with exceptional performance attributes, considering their density range, the absence of intentionally densified surface layers, and without additional water repellents or enhancers.

The study validated the hypothesis that ester linkages between CA's carboxyl groups and the OH groups of hemp carbohydrates played a crucial role in bonding in CA-ULHPB. The significant involvement of lignin during the formation of CA-ULHPB indicated that CA reacted not only with carbohydrates but also with the OH groups of both aromatic and aliphatic components of lignin. The observed internal rearrangement of lignin may be attributed to the formation of pseudo-lignin.

Additionally, optimising panel compositions and processing parameters demonstrated the notable influence of particle size mix (PSM) on panel properties, such as expansion, internal bond strength (IB), water absorption (WA), and thickness swelling (TS). These findings provide valuable insights for optimising CA-ULHPB production.

While variations in CA content and pressing time had a notable impact on TS and WA, the dimensional stability of the panels was not significantly affected by PSM in variants with low CA content and shorter pressing times. The research also indicated that CA-ULHPB met moisture-resistant particleboard specifications outlined in AS/NZS 1859.1 for variants with greater CA content and longer pressing times.

Future studies should explore improved adhesive mechanisms, thermal pre-treatments of the raw material, and lamination substrates to enhance the flexural capacity and expand the potential application range of CA-ULHPB. This may include evaluating acoustic and thermal

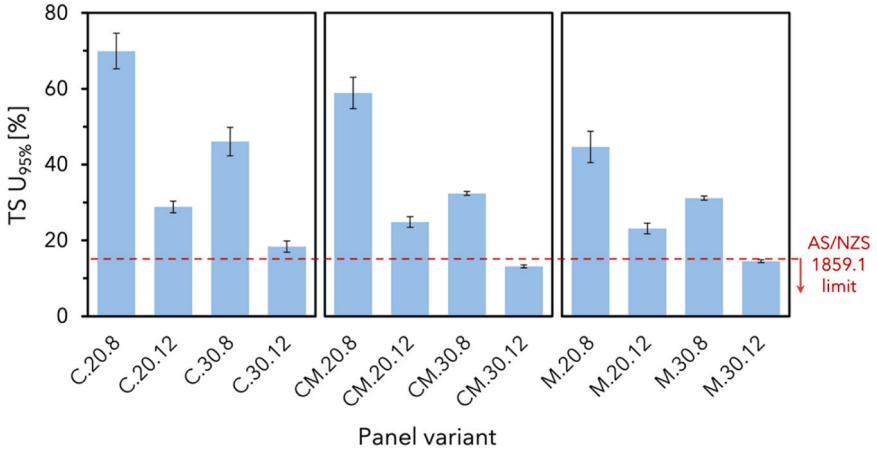

Fig. 10. Comparison of thickness swelling upper 95-percentile values (TS $U_{95\%}$). C = 100% coarse, CM = 50% coarse and 50% medium, M = 100% medium, 20 and 30 = citric acid content (%), 8 and 12 = pressing time (min).

insulation properties, fire resistance, recyclability, and biodegradability. Ultimately, this study's positive outcomes underscore the potential for creating biobased lightweight hemp particleboard, which could serve as core layers in innovative sandwich composites. While the properties of CA-ULHPB require further development and enhancement, it is feasible to imagine their use extending beyond furniture and cabinetry, serving as components for non-loadbearing applications in modular construction systems or integration into quickly deployable emergency units.

Utilising systematically recovered hemp hurd and a natural, formaldehyde-free binder like CA, offers an environmentally responsible alternative to traditional building materials. This approach not only addresses concerns about resource scarcity but also aligns with the principles of the circular economy.

Funding

This research was funded by the Australian Government through the Australian Centre for International Agricultural Research (ACIAR) program, Project No. FST/2016/151. The main author was provided with a financial contribution from The Dr. Albert Shimmins Fund.

CRediT authorship contribution statement

Fehrmann Johannes: Conceptualization, Data curation, Formal analysis, Investigation, Methodology, Project administration, Software, Validation, Visualization, Writing – original draft, Writing – review & editing. **Ismayati Maya:** Investigation, Writing – review & editing. **Dwianto Wahyu:** Resources, Writing – review & editing. **Belleville Benoit:** Conceptualization, Funding acquisition, Project administration, Resources, Supervision, Validation, Writing – review & editing. **Ozarska Barbara:** Conceptualization, Funding acquisition, Project administration, Resources, Supervision, Validation, Writing – review & editing.

Declaration of Generative (AI) and AI-assisted technologies in the Writing Process

During the preparation of this work the author(s) used ChatGPT-3.5 (3/8/2023) in order to improve readability and language. After using this tool/service, the author(s) reviewed and edited the content as needed and take(s) full responsibility for the content of the publication.

Declaration of Competing Interest

The authors declare that they have no known competing financial interests or personal relationships that could have appeared to influence the work reported in this paper.

Data availability

Data will be made available on request.

Acknowledgement

The authors acknowledge the contribution of Darren Christie (Australian Hemp Manufacturing Company, VIC) for providing decorticated Frog1 hemp hurd chips.

References

Alao, P., Tobias, M., Kallakas, H., Poltimäe, T., Kers, J., Goljandin, D., 2020. Development of hemp hurd particleboards from formaldehyde-free resins. Agron. Res. 18 (Special Issue 1), 679–688. https://doi.org/10.15159/ar.20.127.

Amirou, S., Pizzi, A., Delmotte, L., 2017. Citric acid as waterproofing additive in butt joints linear wood welding. Eur. J. Wood Wood Prod. 75 (4), 651–654. https://doi.org/10.1007/s00107-017-1167-x.

Ando, D., Umemura, K., 2021. Bond structures between wood components and citric acid in wood-based molding. Polymers 13 (1), 58.

ANSI. *A208.1–1999 - Particleboard*. Composite Panel Association. 1999.

Apelblat, A., 2014. CITRIC ACID. Springer, Cham. https://doi.org/10.1007/978-3-319-11233-6.

AS/NZS 1859.1. Reconstituted wood-based panels - Specifications. Part 1: Particleboard. Sydney, Australia: SAI Global. 2017.

AS/NZS 4266.1. Reconstituted wood-based panels - Methods of testing. Part 1: Base panels. Sydney, Australia: SAI GLobal. 2017.

Ashori, A., Nourbakhsh, A., 2008. Effect of press cycle time and resin content on physical and mechanical properties of particleboard panels made from the underutilized low-quality raw materials. Ind. Crops Prod. 28 (2), 225–230. https://doi.org/10.1016/j.indcrop.2008.02.015.

Bavaneghi, F., Ghorbani, M., 2015. Mechanical behavior and springback of acetylated particleboard made in different press times. Wood Mater. Sci. Eng. 11 (1), 57–61. https://doi.org/10.1080/17480272.2015.1006249.

Belleville, B., Koumba-Yoya, G., Stevanovic, T., 2018. Effect of Wood Welding Process on Chemical Constituents of Australian Eucalyptus. J. Wood Chem. Technol. 39 (1), 43–56. https://doi.org/10.1080/02773813.2018.1494745.

Burnett, M.P., Kharazipour, A., 2017. Mechanical behaviour of a lightweight, three-layered sandwich panel based on the raw material maize. Holzforsch 72 (1), 65–70. https://doi.org/10.1515/hf-2017-0028.

Chen, M., Zheng, S., Wu, J., Xu, J., 2023. Study on preparation of high-performance binderless board from Broussonetia papyrifera. J. Wood Sci. 69 (1) https://doi.org/10.1186/s10086-023-02092-3.

Cosereanu, C., Brenci, L.M., Zeleniuc, O., Fotin, A., 2015. Effect of particle size and geometry on the performance of single-layer and three-layer particleboard made from sunflower seed husks. BioResources 10 (1), 1127-1136. https://doi.org/10.15376/biores.10.1.1127-1136.

Del Menezzi, C., Amirou, S., Pizzi, A., Xi, X., Delmotte, L., 2018. Reactions with wood carbohydrates and lignin of citric acid as a bond promoter of wood veneer panels. Polym. (Basel) 10 (8). https://doi.org/10.3390/polym10080833.

Delhomme, F., Hajimohammadi, A., Almeida, A., et al., 2020. Physical properties of Australian hurd used as aggregate for hemp concrete. Mater. Today Commun. 24 https://doi.org/10.1016/j.mtcomm.2020.100986.

Dunky, M., Pizzi, A., 2002. Chapter 23 - Wood adhesives. In: Dillard, D.A., Pocius, A.V., Chaudhury, M. (Eds.), Adhesion Science and Engineering Surfaces, Chemistry and Applications. Elsevier Science & Technology, pp. 1039–1103. https://doi.org/10.1016/B978-044451140-9/50023-8.

FAO, 2022. Global forest sector outlook 2050: Assessing future demand and sources of timber for a sustainable economy – Background paper for The State of the World's Forests 2022, 31. Accessed 22.2.2023. https://www.fao.org/documents/card/en/c/cc2265en.

EWPAA. FACTS ABOUT PARTICLEBOARD AND MDF Australian Wood Panels Association Incorporated. 2008. https://ewp.asn.au/.

Fehrmann J., Belleville B., Ozarska B., Ismayati M., Dwianto W. Association of hemp hurd (Cannabis sativa L.) cultivar and processing on thermo-chemical properties. *(in press)*. 2023b:

Fehrmann, J., Belleville, B., Ozarska, B., 2022. Effects of particle dimension and constituent proportions on internal bond strength of ultra-low-density hemp hurd particleboard. Forests 13 (11), 1967. https://doi.org/10.3390/f13111967.

Fehrmann, J., Belleville, B., Ozarska, B., Gutowski, W.S., Wilson, D., 2023a. Influence of particle granulometry and panel composition on the physico-mechanical properties of ultra-low-density hemp hurd particleboard. Polym. Compos. https://doi.org/10.1002/pc.27631.

Ferrandez-Garcia, M.T., Ferrandez-Garcia, C.E., Garcia-Ortuño, T., Ferrandez-Garcia, A., Ferrandez-Villena, M., 2019. Experimental evaluation of a new giant reed (*Arundo donax l.*) composite using citric acid as a natural binder. Agronomy 9 (12), 882. https://doi.org/10.3390/agronomy9120882.

Ferrandez-Garcia, M.T., Ferrandez-Garcia, A., Garcia-Ortuño, T., Ferrandez-Garcia, C.E., Ferrandez-Villena, M., 2020. Influence of particle size on the properties of boards made from washingtonia palm rachis with citric acid. Sustainability 12 (12). https://doi.org/10.3390/su12124841.

Gordon S., Miao M. *Developing technical plans for processing Australian industrial hemp straw*. AgriFutures Australia. 2022. https://agrifutures.com.au/related-projects/developing-technical-plans-for-processing-australian-industrial-hemp-straw/.

Halpern, J.M., Urbanski, R., Weinstock, A.K., Iwig, D.F., Mathers, R.T., von Recum, H.A., 2014. A biodegradable thermoset polymer made by esterification of citric acid and glycerol. J. Biomed. Mater. Res A 102 (5), 1467–1477. https://doi.org/10.1002/jbm.a.34821.

Hu, F., Jung, S., Ragauskas, A., 2012. Pseudo-lignin formation and its impact on enzymatic hydrolysis. Bioresour. Technol. 117, 7–12. https://doi.org/10.1016/j.biortech.2012.04.037.

Kawai, S., Sasaki, H., 1993. Low-Density Particleboard. In: Shiraishi, N., Kajita, H., Norimoto, M. (Eds.), Recent Research on Wood and Wood-Based Materials. Elsevier, pp. 33–41. https://doi.org/10.1016/B978-1-4831-7821-9.50009-5.

Kelly, M.W., 1977. Critical Literature Review of Relationships Between Processing Parameters and Physical Properties of Particleboard. Forest Products Laboratory, Forest Service, US Department of Agriculture. *General Technical Report FPL-10*.

Khojasteh-Khosro, S., Shalbafan, A., Thoemen, H., 2020. Preferences of furniture manufacturers for using lightweight wood-based panels as eco-friendly products. /05/01 2020 Eur. J. Wood Wood Prod. 78 (3), 593–603. https://doi.org/10.1007/s00107-020-01519-8.

Kirilovs, E., Zotova, I., Kukle, S., Pugovičs, K., 2021. Low density hemp shive particleboards for latent thermal energy storage performance. J. Energy Syst. 5 (5), 1–9. https://doi.org/10.30521/jes.805791.

Kurkowiak, K., Hentges, D., Dumarçay, S., Gérardin, P., Militz, H., 2022. Understanding the mode of action of sorbitol and citric acid (SorCA) in wood. Wood Mater. Sci. Eng. 1–9. https://doi.org/10.5658/WOOD.2017.45.4.43.

Kusumah, S.S., Umemura, Ki, Yoshioka, K., Miyafuji, H., Kanayama, K., 2016. Utilization of sweet sorghum bagasse and citric acid for manufacturing of particleboard I: effects of pre-drying treatment and citric acid content on the board properties. Ind. Crops Prod. 84, 34–42. https://doi.org/10.1016/j.indcrop.2016.01.042.

Kusumah, S.S., Umemura, K., Guswenrivo, I., Yoshimura, T., Kanayama, K., 2017. Utilization of sweet sorghum bagasse and citric acid for manufacturing of particleboard II: influences of pressing temperature and time on particleboard properties. J. Wood Sci. 63 (2), 161–172. https://doi.org/10.1016/j.indcrop.2016.01.042.

Lee, S.H., Md Tahir, P., Lum, W.C., et al., 2020. A review on citric acid as green modifying agent and binder for wood. Polymers 12 (8), 1692. https://doi.org/10.3390/polym12081692.

Li, X., Cai, Z., Winandy, J.E., Basta, A.H., 2010. Selected properties of particleboard panels manufactured from rice straws of different geometries. /06/01/ 2010 Bioresour. Technol. 101 (12), 4662–4666. https://doi.org/10.1016/j.biortech.2010.01.053.

Li, Y., Hu, C., Tu, D., Chen, R., Yun, H., 2023. Utilization of lychee pruning timber as alternative raw materials for manufacturing tubular particleboard. Ind. Crops Prod. 203 https://doi.org/10.1016/j.indcrop.2023.117092.

Liao, R., Xu, J., Umemura, K., 2016. Low density sugarcane bagasse particleboard bonded with citric acid and sucrose: effect of board density and additive content. BioResources 11 (1), 2174-2185.

Maloney, T.M., 1977. Modern Particleboard & Dry-Process Fiberboard Manufacturing. Miller Freeman.

Marbun, S.D., Dwianto, W., Meliala, S.B.P.S., Widyorini, R., Augustina, S., Hiziroglu, S., 2023. Dimensional stability mechanisms of binderless boards by heat or steam treatment: a review. /08/22 2023 Cellulose. https://doi.org/10.1007/s10570-023-05429-9.

de Melo, R.R., Santini, E.J., Haselein, C.R., Stangerlin, D.M., 2009. Properties of wood and rice husk particleboard in different proportions. Ciência Florest., St. Maria 19 (4), 449–460. https://doi.org/10.5902/19805098899.

Mert, Y., Zeki, C., Oktay, G., 2022. Chemical performance analysis of nanocellulose/boron-compound-reinforced hybrid UF resin. Green. Mater. 10 (2), 90–96. https://doi.org/10.1680/jgrma.20.00077.

Mert, Y., Zeki, C., Burak, A., Turker, D., 2023. Performance properties of engineered wood composites reinforced by lignosulfonates. Green. Mater. 11 (2), 60–68. https://doi.org/10.1680/jgrma.21.00069.

Mohebby, B., Gorbani-Kokandeh, M., Soltani, M., 2009. Springback in acetylated wood based composites. Constr. Build. Mater. 23 (9), 3103–3106. https://doi.org/10.1016/j.conbuildmat.2009.02.007.

Moldoveanu, S.C., 2019. Chapter 12 - Pyrolysis of Carboxylic Acids. In: Moldoveanu, S.C. (Ed.), Pyrolysis of Organic Molecules (Second Edition). Elsevier, pp. 483–553. https://doi.org/10.1016/B978-0-444-64000-0.00012-3.

National Institute of Standards and Technology. NIST LIBRARY 2017.14. https://chemdata.nist.gov/dokuwiki/doku.php?id=chemdata:start#libraries.

Nemli, G., 01/01 2003. Effects of some manufacturing factors on the properties of particleboard manufactured from alder (Alnus glutinosa subsp. Barbata). *Turk. J. Agric.* . 27, 99–104.

Nitu, I.P., Rahman, S., Islam, N.M., Ashaduzzaman, M., Shams, I.M., 2022. Preparation and properties of jute stick particleboard using citric acid-glycerol mixture as a natural binder. J. Wood Sci. 68 (30), 9. https://doi.org/10.1186/s10086-022-02039-0.

Palardy, R.D., Haataja, B.A., Shaler, S.M., Williams, A.D., Laufenberg, T.L., 1989. Pressing of wood composite panels at moderate temperature and high moisture content. . Prod. J. 39 (4), 27–32.

Petersen, J.-E., Elbersen, B., Wiesenthal, T., Feehan, J., Eppler, U., 2007. Estimating the environmentally compatible bioenergy potential from agriculture. Technical report. European Environment Agency (Accessed 21 April 2020). https://www.eea.europa.eu/publications/technical_report_2007_12.

Picandet, V., 2013. Characterization of Plant-Based Aggregates. In: Amziane, S., Arnaud, L., Challamel, N. (Eds.), Bio-aggregate-based Building Materials. John Wiley & Sons, Inc, pp. 27–74. https://doi.org/10.1002/9781118576809.ch2.

Pizzi, A.P., Papadopoulos, A., Policardi, F., 2020. Wood Composites and Their Polymer Binders, 05/13 Polymers 12. https://doi.org/10.3390/polym12051115.

Randle, P.J., Garland, P.B., Hales, C.N., Newsholme, E.A., 1963. The glucose fatty-acid cycle. Its role in insulin sensitivity and the metabolic disturbances of diabetes mellitus. Lancet 1 (7285), 785–789. https://doi.org/10.1016/s0140-6736(63)91500-9.

Sackey, E.K., Semple, K.E., Oh, S.W., Smith, G.D., 2008. Improving core bond strength of particleboard through particle size redistribution. Article. Wood Fiber Sci. 40 (2), 214–224. DOI: https://api.semanticscholar.org/CorpusID:56369995.

Salami, A., Heikkinen, J., Tomppo, L., et al., 2021. A comparative study of pyrolysis liquids by slow pyrolysis of industrial hemp leaves, hurds and roots. Molecules 26 (11). https://doi.org/10.3390/molecules26113167.

Sam-Brew, S., Smith, G.D., 2017. Flax shive and hemp hurd residues as alternative raw material for particleboard production. BioResources 12 (3), 5715-5735.

Santoso, M., Widyorini, R., Agus Prayitno, T., Sulistyo, J., Hamidah, N., 2020. Effect of pressing temperatures on bonding properties of sucrose-citric acid for nipa palm fronds particleboard. Wood Res 65 (5), 747–756. https://doi.org/10.37763/wr.1336-4561/65.5.747756.

Schramm, C., Rinderer, B., 1999. Influence of additives on the formation of unsaturated PCAs produced during durable-press curing with citric acid. Color. Technol. 115 (10), 306–311. https://doi.org/10.1111/j.1478-4408.1999.tb00384.x.

Schwarzova, I., Stevulova, N., Melichar, T., 2017. Lightweight composites based on technical hemp hurds in construction industry. Chem. Eng. Trans. VOL. 57, 1369–1374. https://doi.org/10.3303/CET1757229.

Shmulsky, R., Jones, P.D., 2011. Forest Products and Wood Science: An Introduction 6ed. Wiley-Blackwell. https://doi.org/10.1002/9780470960035.

de Souza, A.M., Varanda, L.D., Ferro, F.S., et al., 2014. Screw pullout strength in particleboards manufactured with waste of eucalyptus grandis wood specie and oat hulls. Int. J. Comp. Mater. 4 (3), 162–167. https://doi.org/10.5923/j.cmaterials.20140403.02.

Stevulova N., Schwarzova I., Cigasova J., Junak J. Effect of physical treatment of hemp hurds on the properties of biocomposites. 2014: 105–111. https://www.scopus.com/inward/record.uri?eid=2-s2.0–84946571343&partnerID=40&md5=2a1676756b872a465dcde48b2d00ff36.

Suchsland, O., 1959. An analysis of the particleboard process. Mich. State Univ. Agric. Exp. Sta. Bull. 42 (2), 350–372.

Sun, S., Zhao, Z., Umemura, K., 2019. Further exploration of sucrose-citric acid adhesive: synthesis and application on plywood. Polymers 11 (11), 1875. https://doi.org/10.3390/polym11111875.

Sutiawan, J., Hermawan, D., Massijaya, M.Y., et al., 2021. Influence of different hot-pressing conditions on the performance of eco-friendly jabon plywood bonded with citric acid adhesive. Wood Mater. Sci. Eng. 17 (6), 400–409. https://doi.org/10.1080/17480272.2021.1884898.

Sutiawan, J., Hermawan, D., Hadi, Y.S., et al., 2022. Properties of sorghum (Sorghum bicolor) biomass particleboard at different maleic acid content and particle size as potential materials for table tennis blade. Biomass-.-. Conv. Bioref. https://doi.org/10.1007/s13399-022-02525-x.

Syamani F.A., Kusumah S.S., Astari L., Prasetiyo K.W., Wibowo E.S., Subyakto. Effect of pre-drying time and citric acid content on Imperata cylindrica particleboards properties. presented at: IOP Conf. Series: Earth and Environmental Science; 2018; Session 209.

Syamani, F.A., Sudarmanto, Subyakto, Subiyanto, B., 2020. High quality sugarcane bagasse-citric acid particleboards. Presente : IOP Conf. Ser.: Earth Environ. Sci.

Tjeerdsma, B.F., Boonstra, M., Pizzi, A., Tekely, P., Militz, H., 1998. Characterisation of thermally modified wood: molecular reasons for wood performance improvement. /05/01 1998 Holz Roh Werkst. 56 (3), 149–153. https://doi.org/10.1007/s001070050287.

Umemura, K., Ueda, T., Munawar, S.S., Kawai, S., 2012. Application of citric acid as natural adhesive for wood. J. Appl. Polym. Sci. 123 (4), 1991–1996. https://doi.org/10.1002/app.34708.

Umemura, K., Sugihara, O., Kawai, S., 2013. Investigation of a new natural adhesive composed of citric acid and sucrose for particleboard. J. Wood Sci. 59 (3), 203–208. https://doi.org/10.1007/s10086-013-1326-6.

Umemura, K., Sugihara, O., Kawai, S., 2015. Investigation of a new natural adhesive composed of citric acid and sucrose for particleboard II - effects of board density and pressing temperature. J. Wood Sci. 61, 40–44. https://doi.org/10.1007/s10086-014-1437-8.

UN. *World Population Prospects 2022: Summary of Results*. Department of Economic and Social Affairs, Population Division. 2022. Accessed 21.2.2023. https://population.un.org/wpp/Publications/.

UN. *World Urbanization Prospects 2018: Highlights*. Department of Economic and Social Affairs, Population Division. 2018. Accessed 21.2.2023. https://population.un.org/wup/Publications/.

Viel, M., Collet, F., Lanos, C., 2018. Chemical and multi-physical characterization of agro-resources' by-product as a possible raw building material (Article.). Ind. Crops Prod. 120, 214–237. https://doi.org/10.1016/j.indcrop.2018.04.025.

Vineeth, S., Gadhave, R., Gadekar, P., 2019. Nanocellulose applications in wood adhesives—review. Open J. Polym. Chem. 9, 63–75. https://doi.org/10.4236/ojpchem.2019.94006.

Vukusic, S.B., Katovic, D., Schramm, C., Trajkovic, J., Sefc, B., 2006. Polycarboxylic acids as non-formaldehyde anti-swelling agents for wood. Holzforsch 60 (4), 439–444. https://doi.org/10.1515/HF.2006.069.

Wibowo, E.S., Kusumah, S.S., Subyakto, Umemura, K., 2021. Modification of novel bio-based adhesive made from citric acid and sucrose by ZnCl2. Int. J. Adhes. Adhes. 108 https://doi.org/10.1016/j.ijadhadh.2021.102866.

Wyrzykowski, D., Hebanowska, E., Nowak-Wiczk, G., Makowski, M., Chmurzyński, L., 2010. Thermal behaviour of citric acid and isomeric aconitic acids. J. Therm. Anal. Calorim. 104 (2), 731–735. https://doi.org/10.1007/s10973-010-1015-2.

Yang, M., Xing, J., Liu, Y., Liu, Y., Mu, T., Zhou, J., 2015. Formation and characterisation of pseudo-lignin microspheres during high-pressure water pretreatment. BioResources 10 (4), 8474-8486.

Zhao, Z., Sakai, S., Wu, D., et al., 2019. FurthEr Exploration of Sucrose–citric Acid Adhesive: Investigation of Optimal Hot-pressing Conditions for Plywood and Curing Behavior. Polymers 11 (12), 1996. https://doi.org/10.3390/polym11121996.

Zvirgzds, K., Kirilovs, E., Kukle, S., Gross, U., 2022. Production of particleboard using various particle size hemp shives as filler. Materials 15 (3), 886. https://doi.org/10.3390/ma15030886.